A.I. KURCHAK

V. Lashkaryov Institute of Semiconductor Physics, Nat. Acad. of Sci. of Ukraine
(41, Prosp. Nauky, Kyiv 03028, Ukraine; e-mail: teoretyk0706@gmail.com)

IMPACT OF THE DOMAIN STRUCTURE IN FERROELECTRIC SUBSTRATE ON GRAPHENE CONDUCTANCE

UDC 539

The review is devoted to the recent theoretical studies of the impact of the domain structure of a ferroelectric substrate on the graphene conductance. An analytical description of the hysteresis memory effect in a field effect transistor based on graphene-on-ferroelectric, taking into account absorbed dipole layers on the free surface of graphene and localized states on its interfaces is considered. The aspects of the recently developed theory of p–n junctions conductivity in a graphene channel on a ferroelectric substrate, which are created by a 180-degree ferroelectric domain structure, are analyzed, and the cases of different current regimes from ballistic to diffusion one are considered. The influence of size effects in such systems and the possibility of using the results for improving the characteristics of field effect transistors with a graphene channel, nonvolatile ferroelectric memory cells with random access, sensors, as well as for the miniaturization of various devices of functional nanoelectronics are discussed.

K e y w o r d s: graphene-on-ferroelectric, domain structure, conductance, field effect transistor.

1. Introduction

Experimental and theoretical studies of the remarkable electromechanical, electrophysical, and transport properties of graphene remain on the top of researchers' attention since the graphene discovery [1,2] till nowadays (see, e.g., [3–5]). A promising and quite feasible way toward the understanding of and control over the graphene-based devices (as well as the devices utilizing other 2D semiconductors) is to use "smart" substrates with additional (electromechanical, polar, and/or magnetic) degrees of functionality. For instance, graphene on a ferroelectric substrate [6–10], whose spontaneous polarization and domain structure can be controlled by an external electric field [11, 12], can be proposed as such "smart" system [13].

The review is organized as following. Section II analyzes our recent theoretical works devoted to changes of the graphene channel conductivity caused by p–n junctions induced by the existence of a single domain wall in a ferroelectric substrate and discusses the various regimes of current and rectification effects. Section III is devoted to the discussion and analysis of the theory of hysteretic phenomena in graphene-on-ferroelectric. Section IV analyzes the dynamics of p–n junctions in a graphene channel induced by the motion of ferroelectric domain walls. Section V considers the possibilities of the graphene separation and stretching induced by the piezoelectric effect of ferroelectric domains. Section VI presents a brief summary of the results.

2. Conductivity of the Graphene Channel with a p–n Junction on the Ferroelectric Domain Wall

The presence of a domain structure in a ferroelectric substrate can lead to the formation of p–n junctions in graphene [11, 12], which are located above the domain walls in a ferroelectric substrate [14–18]. Note that the unique properties of the p–n junction in graphene have been realized much earlier by the multiple gates doping of a graphene channel by electrons or holes, respectively [19–21]. Then they have been studied theoretically [22, 23] and experimentally [24–26]. Hinnefeld et al. [11] and Baeumer et al. [12] created a p–n junction in graphene using ferroelectric substrates by imposing a graphene sheet on a 180°-ferroelectric domain wall (**FDW**). Due to the charge separation by an electric field of a FDW – surface junction, p–n junctions occur in graphene [27, 28].

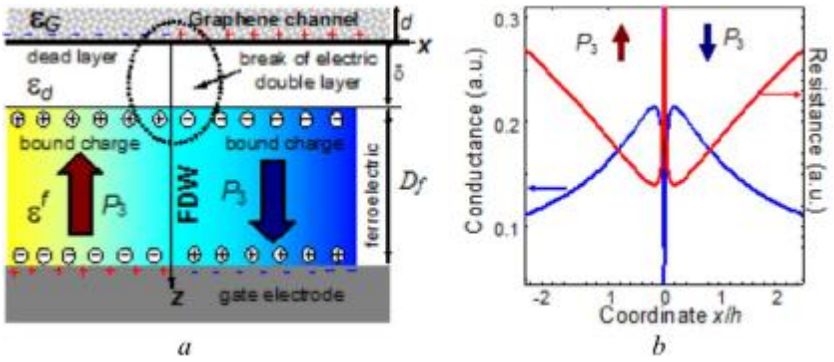

Fig. 2.1. 180°-FDW structure near the ferroelectric surface in the graphene-on-ferrroelectric. The discontinuity of the electric double layer consisting of the screening and bound charges creates a depolarization electric field that penetrates into the gap (*a*). Graphene conductance (left vertical axis) and resistance (right vertical axis) x-distributions caused by the FDW located at $x = 0$ in the graphene-on-ferrroelectric heterostructure (*b*). (Reproduced from [A.N. Morozovska, E.A. Eliseev, M.V. Strikha. *Appl. Phys. Lett.* **108**, 232902 (2016)], with the permission of AIP Publishing)

Note that the elastic strain can change the band structure of graphene (e.g., via the deformation potential) and open the band gap [4, 5, 29–31]. We have shown [18] that the piezoelectric displacement of the ferroelectric domain surfaces can lead to the stretching and separation of graphene areas at the steps between elongated and contracted domains. Graphene separation at FDWs induced by piezoeffect can cause an increase of the graphene channel conductance. Below, we briefly review the results of Refs. [14–18] and discuss their correlation with available experimental and other theoretical works.

Semiquantum and semiphenomenological analytical models have been developed for different types of carrier transport (ballistic, diffusive, *etc.*) in a single-layer graphene channel at 180°-FDW [14, 15].

Specifically, the influence of a ferroelectric domain wall on the ballistic conductance of a graphene channel has been studied in the Wentzel–Kramers–Brillouin (WKB) approximation in Ref. [14]. Here, we consider the graphene channel separated from a ferroelectric layer with the FDW structure by an ultra-thin dielectric layer (a physical gap or a ferroelectric dead layer). The ferroelectric layer makes an ideal electric contact with the gate electrode (see Fig. 2.1, *a*).

A pronounced broadening of the FDW near the surface appears [14, 32] in order to decrease the depolarization electric field produced by the uncompensated polarization bound charges localized in a thin sub-surface layer of ferroelectric. Despite the broadening, the stray electric field is still strong enough to induce the p–n junction in the graphene channel. A potential barrier for electrons and holes emerges in the p–n junction, when a positive (negative) voltage is applied to the left (right) contact of the channel. The probability w for an electron in the n-region with the wave vector k directed at the angle ϑ with respect to the x axis to pass into the p-region can be calculated using the scheme presented in Ref. [33]. With an allowance for the linear graphene band spectrum

$$E(k_x, k_y) = v_{\mathrm{F}}\hbar\sqrt{k_x^2 + k_y^2},$$

at the junction center, $x = 0$, electron's kinetic energy equals $v_{\mathrm{F}}\hbar\sqrt{k_x^2 + k_y^2}$, where the momentum y-component $k_y = k_{\mathrm{F}} \sin\vartheta$ is conserved ($v_{\mathrm{F}} \approx 10^6$ m/s is the so-called Fermi velocity of the electron, it is determined by the energy of σ-bonds between carbon atoms in the graphene plane, Ref. [3]). Therefore, the $x$component is determined by the expression

$$k_x(x) = \sqrt{(e\varphi(x,0)/v_{\mathrm{F}}^{\hbar})^2 - (k_{\mathrm{F}} \sin\vartheta)^2}.$$

The classically allowed region of electron motion is determined by the inequality $e\varphi(x,0) > v_{\mathrm{F}}\hbar k_y$, which means that the electron cannot overpass the turning point at the distance l_x from the center of the junction located at the FDW.

For small angles $|\vartheta| \ll 1$, the probability w can be estimated quasiclassically in the WKB approximation as $w \approx e^{-2S/\hbar}$, where $S = i\hbar \int_{-l_x}^{l_x} k_x(x)dx$. The conductance *per p–n junction unit width* has been estimated as [14]:

$$G_{pn}^{\text{ball}} \approx \frac{e^2 k_{\text{F}}}{2\pi^2\hbar}\sqrt{\frac{\pi}{P_x}}. \tag{2.1}$$

In Eq. (2.1),

$$k_{\text{F}} = \frac{\pi^2\varepsilon_0\varepsilon_{33}^{\text{f}}}{e^2}\frac{\hbar v_{\text{F}} Q}{\delta^* \ln 3}$$

is the Fermi wave vector, Q is the dimensionless factor

$$Q = \frac{e\,(P_S/\varepsilon_0)}{\varepsilon_{33}^{\text{f}} + \gamma\,\varepsilon_{\text{d}}}\frac{2\gamma\delta^* \ln 3}{\pi\hbar k_{\text{F}} v_{\text{F}}}$$

and

$$P_x \approx \pi^3\varepsilon_0\varepsilon_{33}^{\text{f}}\hbar w_{\text{F}}/e^2$$

is the probability factor. The spontaneous polarization isP_S, $e$is an electron charge, ε_0 is the universal dielectric constant, the relative permittivity of the dielectric layer ε_{d} is equal either to the background permittivity of ferroelectric for the dead layer or to unity for the physical gap; $\gamma = \sqrt{\varepsilon_{33}^{\text{f}}/\varepsilon_{11}^{\text{f}}}$ is the anisotropy factor of ferroelectric, $\varepsilon_{ii}^{\text{f}}$ are components of the relative permittivity of a ferroelectric substrate, ($\varepsilon_{33}^{\text{f}}$ is the permittivity of ferroelectric along the z direction, which is normal to the graphene plane, $\varepsilon_{11}^{\text{f}}$ is the permittivity of ferroelectric along the channel x-direction); δ^* is the sum of the thickness δ of the dielectric layer and the effective screening length of graphene [14], [34]].

The wave vector $k_{\text{F}} \equiv \sqrt{\pi n_{2\text{D}}}$, (2.1) can be rewritten as [14]:

$$G_{pn}^{\text{ball}} \cong \frac{e^2}{\pi\hbar}\sqrt{\frac{\alpha}{\varepsilon_{33}^{\text{f}}}\frac{c}{\pi v_{\text{F}}}n_{2\text{D}}}. \tag{2.2}$$

Here, $\alpha = e^2/4\pi\varepsilon_0\,(\hbar c)$ is the fine-structure constant, and c the light velocity in vacuum. To within a dimensionless factor $\alpha = e^2/4\pi\varepsilon_0\,(\hbar c) \sim 0.1$, Eq. (2.2) coincides with the bookish expression for the ballistic conductivity of graphene per unit channel width, $\sigma = 2e^2\sqrt{n_{2\text{D}}}/\hbar$ [3, 35]. However, Eq. (2.2) differs from Eq. (2) in [33], because, in graphene-on-ferroelectric, the concentration of 2D-carriers in graphene $n_{2\text{D}}$ is governed by the spontaneous polarization of ferroelectric,

$$n_{2\text{D}}\,(x) \approx \frac{2\gamma\varepsilon_{33}^{\text{f}}\,(P_S/e)}{\varepsilon_{33}^{\text{f}} + \gamma\,\varepsilon_{\text{d}}}.$$

The nominal resistance R_{np} is inversely proportional to conductance (2.2), i.e. $R_{np} = 1/(WG_{pn}^{\text{ball}})$, where $W$is the p–n junction width.

The conductivity and resistivity redistributions caused by the FDW are shown in Fig. 2.1, *b*. As one can see, the width of the p–n junction region is about $2h$. Since $\sigma_0 = e^2/(2\pi\hbar)$ is a quantum of conductance, the ratio $WG_{pn}^{\text{ball}}/\sigma_0$ gives us the idea of the number of conductivity modes. This result coincides by order with that calculated in [36].

The estimation of the concentration caused by ferroelectric dipoles leads to values of about 10^{19} m^{-2} that is two orders of magnitude higher than for the highest one possible for gated graphene on the SiO_2 substrate (this limit is determined by the dielectric breakdown field). Therefore, the graphene p–n junction at the FDW would be characterized by rather a high ballistic conductivity and a low resistivity. However, the presence of the factor $1/(\varepsilon_{33}^{\text{f}})^{1/2}$in (2.2), where $\varepsilon_{33}^{\text{f}}$can be rather high for the ferroelectric substrate, for the conductance of the p–n junction for the direct polarity of a voltage on S and D electrodes (electron is moving through the barrier of the p–n-junction), on the one hand, and the absence of this factor for the opposite polarity (electron doesn't feel the barrier, while moving in the opposite direction), on the other hand, laed to that the graphene p–n junction at the ferroelectric domain would be an excellent rectifier with a conductivity ratio of about 10 between the direct and reverse polarities of an applied voltage.

However, the majority of realistic graphene devices are described by the mean free path of electrons $\lambda \sim$ (50–250) nm and so are operating in a diffusive regime [15]. Since the electron mean free path λ in graphene channel is usually much longer than the intrinsic thickness w of the uncharged domain wall in proper ferroelectric, that is about 1–10 nm [37], one can divide the graphene channel with length L between the source and the drain into 3 sections: one, containing a p–n junction itself, with length λ, and the two others, on both sides from the junction, with the total length $L - \lambda$ (see Fig. 2.2).

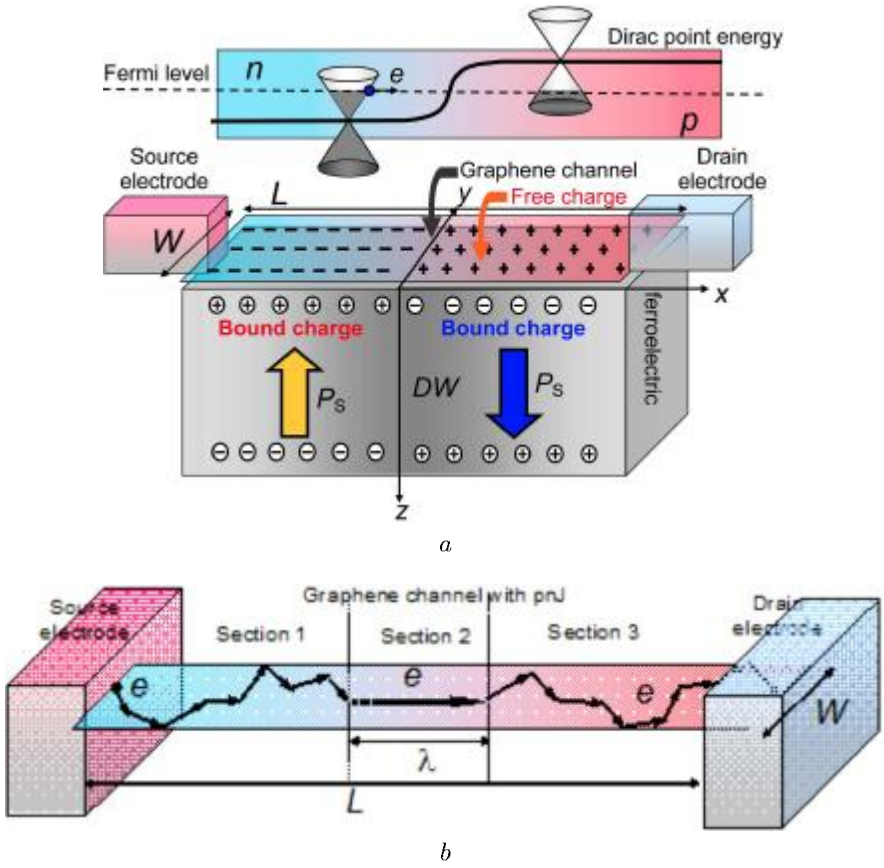

Fig. 2.2. (*a*) 180°-FDW structure near the uniaxial ferroelectric surface in the graphene-on-ferroelectric heterostructure (bottom part) and the potential barrier of the *p*–*n* junction (pnJ) for an electron (upper part). Single-layer GC length is L, its width is W. Ferroelectric substrate with polarizations $\pm P_S$ separated by a 180°-FDW is thick enough. (*b*) Formal division of the graphene channel with a pnJ into three sections. The current in sections 1 and 3 is diffusive, while, in section 2, it is ballistic. (Reproduced from [M.V. Strikha, A.N. Morozovska. *J. Appl. Phys.* **120**, 214101 (2016)], with the permission of AIP Publishing)

The total conductance of the sample is governed by the evident expression [15]

$$\frac{1}{G^{\text{total}}} = \frac{1}{W}\left(\frac{1}{G^{\text{diff}}} + \frac{1}{G^{\text{ball}}}\right). \tag{2.3}$$

As anticipated, the conductance is proportional to the graphene channel width W and the bookish relationship

$$G^{\text{diff}} = \frac{\lambda}{L+\lambda} G^{\text{ball}}$$

is valid (see, e.g., Refs. [40, 51]). The change of the voltage polarity on contacts does not change the conductance of sections 1 and 3. On the contrary, the unit length conductance of section 2 is described in these cases by different expressions,

$$G^{\text{ball}} = \frac{2e^2}{\hbar\pi^{3/2}}\sqrt{n_{2\text{D}}}$$

and

$$G^{\text{ball}}_{pn} \cong \frac{e^2}{\pi\hbar}\sqrt{\frac{\alpha}{\varepsilon^{\text{f}}_{33}}\frac{c}{\pi v_{\text{F}}}n_{2\text{D}}}$$

(see Eq. (2.2) and Ref. [15]), and the permittivity $\varepsilon^{\text{f}}_{33}$ of ferroelectric along the direction normal to the graphene plane can be rather high (~500 for PZT or even much higher ~5000 for the relaxor ferroelectric). Thus, the ratio of conductances for different polarities is:

$$\frac{G^{\text{total}}_{+}}{G^{\text{total}}_{-}} = \frac{\beta(L+\lambda)}{\beta(L+\lambda)+\lambda}. \tag{2.4}$$

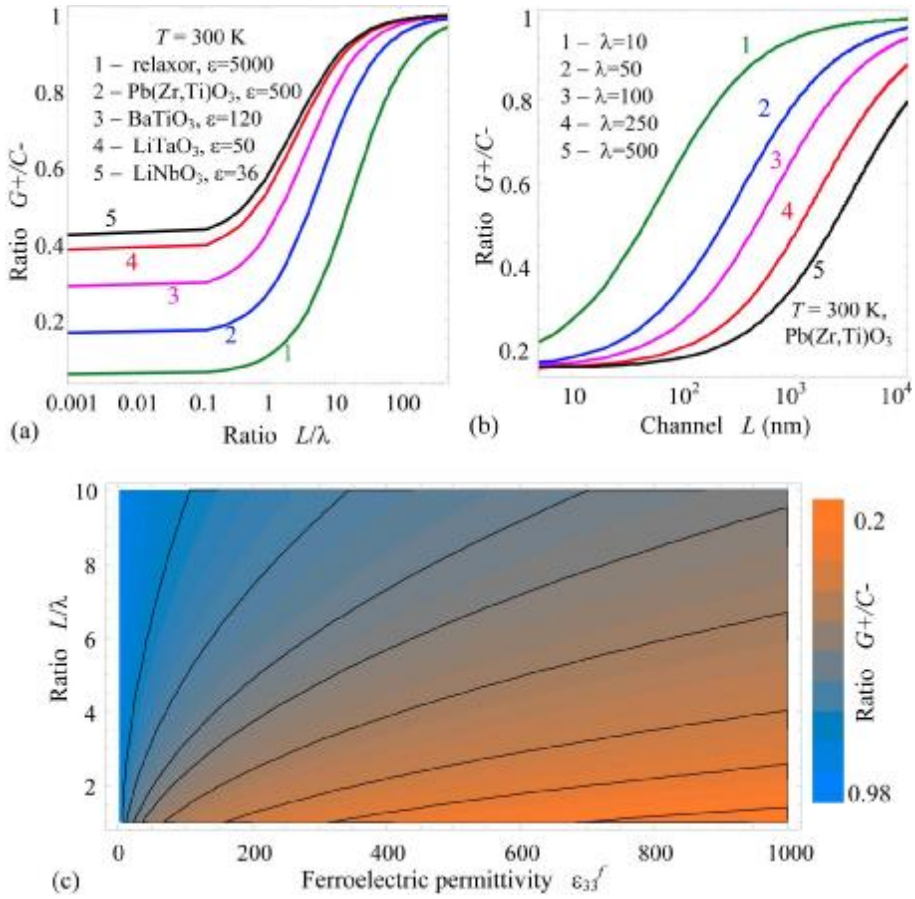

Fig. 2.3. (*a*) The ratio of the pnJ total conductances for opposite polarities of applied voltages, $G_+^{\rm total}/G_-^{\rm total}$, as a function of the ratio of the graphene channel length to the mean path, L/λ calculated from Eq. (11) for different ferroelectric substrates, namely, for several $\beta(\varepsilon_{33}^{\rm f})$, where the dielectric permittivity $\varepsilon_{33}^{\rm f} \geqslant 5000$ for the ferroelectric relaxor, 500 for Pb(Zr, Ti)O_3, 120 for $BaTiO_3$, 50 for $LiTaO_3$, and 36 for $LiNbO_3$ at room temperature 300 K (curves *1–5*). (*b*) The ratio $G_+^{\rm total}/G_-^{\rm total}$ as a function of the graphene channel length L calculated for several mean paths $\lambda = (10, 50, 100, 250, 500)$ nm (curves *1–5*) for ferroelectric Pb(Zr, Ti)O_3 substrate and $T = 300$ K. (*c*) Contour map of the ratio $G_+^{\rm total}/G_-^{\rm total}$ in the coordinates $\{L/\lambda,\ \varepsilon_{33}^{\rm f}$. Reproduced from [M.V. Strikha, A.N. Morozovska. *J. Appl. Phys.* **120**, 214101 (2016)], with the permission of AIP Publishing

The parameter β depends on the dielectric permittivity,

$$\beta(\varepsilon_{33}^{\rm f}) = \sqrt{\pi\alpha/(4\varepsilon_{33}^{\rm f} v_{\rm F})}$$

and the electron mean free path λ depends on the concentration $n_{\rm 2D}$, and, so, on the ferroelectric polarization, since $n_{\rm 2D} \sim \pi(P_S/e)$ [15, 34]. When the scattering of electrons in the graphene channel at charged impurities in ferroelectric is dominant (which is the most common case for real graphene operational devices, see, e.g., [3]),

$$\lambda(n_{\rm 2D}) \sim \sqrt{n_{\rm 2D}}.$$

In the case of the short ballistic channel,

$$L \ll \lambda, \quad \frac{1}{G^{\rm total}} \approx \frac{1}{G^{\rm ball}}.$$

In the opposite limit of the long diffusive channel,

$$L \gg \lambda, \quad \frac{G_+^{\rm total}}{G_-^{\rm total}} = 1$$

and so the rectifying properties of p–n junctions vanish.

The ratio $G_+^{\rm total}/G_-^{\rm total}$ as a function of the ratio L/λ calculated for different ferroelectric substrates (relaxor, Pb(Zr,Ti)O_3, $BaTiO_3$, $LiTaO_3$, and $LiNbO_3$) is presented in Fig. 2.3. As one can see from

Fig. 2.3, small values of $G_{+}^{\text{total}}/G_{-}^{\text{total}}$ can be obtained for the ratios of L/λ of unity order or smaller and ferroelectric substrates with high permittivity. The expected result can be realized for the channels with submicron length in the case of the comparative values of the electron mean free path. The situation corresponds to the current regime transient from the diffusive to ballistic one; we mention that the distance between the parallel FDWs is generally much longer, which enables to fabricate a micron-length channel with contacts near one FDW only. For ferroelectrics with extremely high permittivity, such as relaxors or $PbZr_xTi_{1-x}O_3$ with composition x near the morphotropic phase boundary $x = 0.52$, the $G_{+}^{\text{total}}/G_{-}^{\text{total}}$ ratio can be essentially smaller than 1 in the case of a pronounced diffusive regime of the current as well. This allows us to consider the ultra-high permittivity ferroelectric substrates as excellent candidates for the fabrication of novel rectifiers based on the graphene p–n junction.

3. Hysteretic Phenomena in Graphene-on-Ferroelectric

3.1. Theoretical formalism

Generally, the dependence of the graphene channel conductivity on the gate voltage is considered to be excellently symmetric,

$$G(V_g) = G(-V_g)$$

(Ref. [3]). This occurs, however, for the specially treated high quality graphene surfaces only. In many real imperfect structures with absorbed dipoles on a free graphene centers, localized states at graphene-substrate interface, *etc.*, this symmetry vanishes. Moreover, the dependence of $G(V_g)$ can get a hysteretic form (see, e.g., Refs. [63–65] and Reviews [66, 67]). This hysteresis can have opposite directions of its loop and needs a special treatment with allowance for different rival physical factors.

Let us consider a conducting graphene channel placed on a dielectric or ferroelectric substrate (see Ref. [16] and Fig. 3.1). The concentration of 2D carriers in the channel is governed by several factors, which are a time-dependent gate voltage $V_g(t)$, polarization of the ferroelectric substrate dipoles, polarization of dipoles (e.g., absorbed water molecules) on graphene surface, and the trapped charge carriers localized at the graphene-substrate interface. The subsequent theoretical formalism is taken from Ref. [16].

From all the abovementioned factors, the graphene channel resistivity can be presented as [16]:

$$\rho\left[V_g, P_s, P_f, T\right] \approx \frac{1}{\sigma\left(V_g, P_s, P_f, T\right)} + \frac{1}{\sigma_{\text{intr}}\left(T\right)} + \frac{1}{\sigma_{\min}}, \tag{3.1}$$

where $P_s\left(t\right)$ is the polarization of dipoles absorbed on the graphene surface, and $P_f\left(t, T\right)$ is the temperature-dependent ferroelectric polarization. For the usual case of graphene under ambient conditions, the scattering of ionized impurities by a substrate dominates [38]. So, the conductivity of the 2D graphene channel is

$$\sigma\left(V_g, P_s, P_f, T\right) = e\mu\, n\left(V_g, P_s, P_f, T\right),$$

where $n\left(V_g, P_s, P_f\right)$ is the 2D carriers concentration per unit area, caused by the gate mixed doping, and by the dipoles absorbed by the surface, as well as by ferroelectric dipoles; μ is the carriers mobility. The second term in Eq. (3.1) is the intrinsic graphene conductivity,

$$\sigma_{\text{intr}}\left(T\right) = e\,\mu n_{\text{intr}}\left(T\right),$$
$$n_{\text{intr}}(T) = \frac{2(k_{\text{B}}T)^2}{\pi(\hbar v_{\text{F}})^2}.$$

The third term in Eq. (3.1) corresponds to the minimal quantum conductivity, $\sigma_{\min} \approx \frac{4e^2}{\hbar}$, that becomes significant at low T.

The localized states are present at the graphene-substrate interface. In the voltage range $V_g\left(t\right) < V_{T1}$, where V_{T1}corresponds to the situation when the occupation of the interface states with the electrons from the graphene channel starts, $E_{\text{F}}(V_{T1}) = E_{T1}$, the 2D concentration of electrons in the graphene channel is given by the capacitor formula [39, 42],

$$n\left(V_g(t)\right) = \frac{\kappa\, V_g\left(t\right)}{4\,\pi\, e\, d},$$

where κ is the dielectric permittivity of a substrate, and $d$is the substrate thickness. The gate voltage

$$V_{T1} = \frac{4\pi e d}{\kappa}\frac{E_{T1}^2}{\pi\hbar^2 v_{\text{F}}^2}$$

leads to the start of the interface states occupation with electrons from the graphene channel. The voltage

$$V_{T2} = \frac{4\pi e d}{\kappa}\frac{E_{T2}^2}{\pi\hbar^2 v_{\text{F}}^2} + \frac{4\pi e d n_T}{\kappa}$$

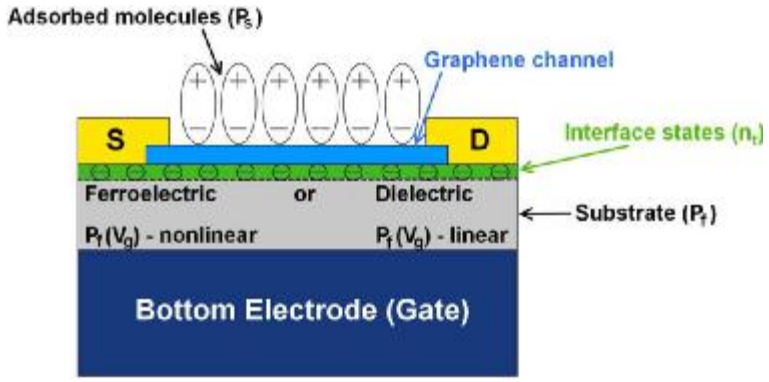

Fig. 3.1. A graphene sheet (channel) placed on a dielectric or ferroelectric substrate. Dipoles (e.g., polar water molecules) can be absorbed by the graphene free surface. Carriers from the channel can be trapped by the centers localized at the graphene-substrate interface. Reproduced from [A.I. Kurchak, A.N. Morozovska, M.V. Strikha. *J. Appl. Phys.* **122**, 044504 (2017)], with the permission of AIP Publishing

corresponds to the situation when all localized interface states are already occupied by electrons from the graphene channel [40].

In the voltage range $V_{T1} \leqslant V_g < V_{T2}$, for which the occupation of interface states occurs,

$$n = \frac{E_{T1}^2}{\pi \hbar^2 v_{\mathrm{F}}^2}.$$

In the voltage range $V_{T2} \leqslant V_g$, where all the interface states are already occupied by electrons, the free electrons' concentration in the channel is governed by the evident relation

$$n\left(V_g\right) = \frac{\kappa\, V_g\left(t\right)}{4\,\pi\, e\, d} - n_T.$$

Let us consider the polarization of dipoles in the ferroelectric substrate and at the graphene surface. If $E_{\mathrm{F}} \leqslant E_{T1}$, similarly to [39, 42], we get:

$$n\left(V_g, P_s, P_f\right) = \frac{\kappa\, V_g\left(t\right)}{4\,\pi\, e\, d} + \frac{P_s\left(t\right) + P_f\left(t, T\right)}{e}. \quad (3.2)$$

The temperature-dependent spontaneous ferroelectric polarization can be described by expression [41]:

$$P_f\left(t,\, T\right) = P_f\left(T\right)\, \tanh\left(s_f\, \left(V_g\left(t\right) - V_c\right)\right), \quad (3.3)$$

where $V_c = E_c\, d$ is a coercive voltage equal to the product of the coercive field and the substrate thickness d, s_f is the "sharpness" of ferroelectric switching. The spontaneous polarization of the dipoles absorbed by the graphene surface is

$$P_s\left(t\right) = P_s \frac{1 - \tanh\left(s_s\, \left(V_g\left(t\right) - V_s\right)\right)}{2}, \quad (3.4)$$

where V_s is the critical voltage that finally destroys the polarization; s_s is a parameter reflecting the "sharpness" of the switching of dipoles. For the backward sweep polarizations, P_f and P_s are

$$P_f\left(t,\, T\right) = P_f\left(T\right)\, \tanh\left(s_f\, \left(V_g\left(t\right) + V_c\right)\right)$$

and

$$P_s(t) = P_s \left[1 - \exp\left(-\frac{t(V_s) - t)}{\tau}\right)\right], \quad (3.5)$$

where $t(V_s)$ is the time moment corresponding to the complete suppression of P_s by the critical gate voltage, τ is the dipoles' relaxation time that can be equal to several seconds [42]. Equations (3.3)–(3.5) are written in the case where the absorbed dipoles recover immediately after the switching to the backward sweep. The above equations are valid in the case where the lifetime of carriers trapped by interface states is much greater than the switching time. The validity of this approximation for graphene on PZT substrate was demonstrated experimentally in Ref. [43].

The nonlinear response of the ideal ferroelectric substrate can be described using the Ginzburg–Landau–Khalatnikov relaxation equation [34, 44, 45]:

$$\Gamma \frac{dP\left(t\right)}{dt} = \alpha\left(T\right) P\left(t\right) + \beta P^3\left(t\right) + \gamma P^5\left(t\right) - E\left(\omega, t\right), \quad (3.6)$$

where α, β, and γ are Landau potential expansion coefficients.

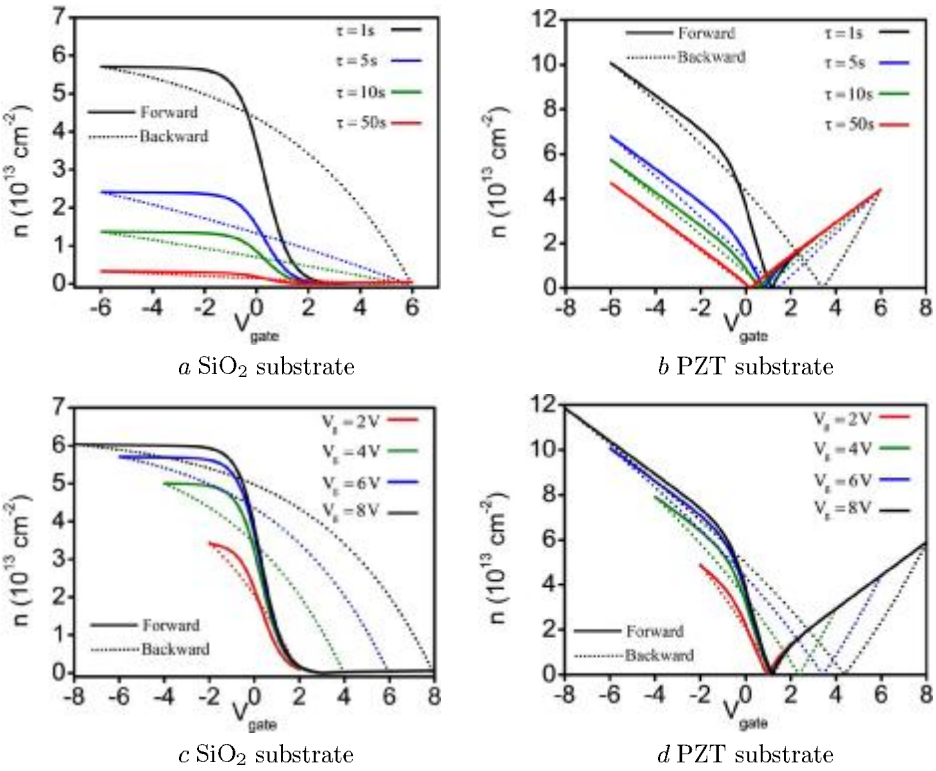

a SiO_2 substrate *b* PZT substrate

c SiO_2 substrate *d* PZT substrate

Fig. 3.2. The dependence of the carrier concentration in the graphene channel on SiO_2 substrate (*a*) and PZT substrate (*b*) vs. the gate voltage calculated for different times τ = 1, 5, 10 and 50 s (different colors) of the surface dipoles relaxation. Forward and backward sweeping dependences are presented by solid and dotted curves, respectively. The time dependence $V_g(t)$ is saw-like with a period $2\pi/\omega$ and the amplitude A. (*c*) The dependence of the carrier concentration in the graphene channel on SiO_2 substrate vs. the gate voltage calculated in different switching ranges for the gate voltage. Forward and backward sweeping dependences are presented by solid and dotted curves, respectively. The curves calculated for different sweeping range $V_g^{\max}$ = ± 2V, ±4V, ±6V, and ±8V, are shown by different colors. (*d*) The dependence of the carrier concentration in the graphene channel on PZT substrate vs. the gate voltage calculated for different relaxation times of surface dipoles. Forward and backward sweeping dependences are presented by solid and dotted curves, respectively. The curves calculated for different dipoles' relaxation times τ = 1, 5, 10, and 50 s are shown by different colors. Reproduced from [A.I. Kurchak, A.N. Morozovska, M.V. Strikha. *J. Appl. Phys.* **122**, 044504 (2017)], with the permission of AIP Publishing

3.2. Gate control of the carrier concentration in the graphene channel

3.2.1. Impact of the surface dipoles on the graphene carriers

The dipoles can be absorbed by the graphene surface (e.g., water molecules studied experimentally in [46–48]), and, in this case, $P_s \neq 0, P_f = 0, n_T = 0$. The dipoles shift the electroneutrality point into the positive range of V_g [16]. So, the graphene channel conductivity is determined by holes at the zero gate voltage. In this case, the carrier concentration in the graphene channel is determined both by the gate doping and by the absorbed dipoles polarization, which, in turn, depends on the external electric field caused by the gate voltage. The estimates [16] showed that the conductivity of the graphene channel would be governed by the time-dependent polarization of dipoles.

Figure 3.2, *a* illustrates the dependence of the carrier concentration on the gate voltage in the graphene channel on a SiO_2 substrate for different times of the surface dipoles relaxation τ. In the initial moment of time (at $V_g = 0$), the graphene channel conductivity is determined by holes, as it was noted before. However, the electric field caused by the gate potential destroys the dipoles polarization at some critical value of V_g. Solid lines correspond to the second forward sweep, i.e. the polarization disappearance after the

first cycle of its recover. The polarization will start to renew at the backward sweep. The value of polarization that recovers within a switching period is different for different relaxation times τ, but it recovers almost completely within a switching period for a short relaxation time. The direction of such hysteresis loop would be opposite to the so-called direct one created by ferroelectric dipoles ("antihysteresis").

Figure 3.2, *c* presents the dependence of the 2D concentration in the graphene channel vs. the gate voltage as a function of the gate voltage switching range. The hysteresis region increases wuth the gate voltage. Considering the direct sweeping (at $dV_g/dt > 0$), the disappearance of surface dipoles' polarization occurs in all ranges of gate voltages at a fixed electric field. After switching the gate voltage in the reverse direction, dipoles' polarization on the graphene surface immediately starts to recover (see dotted lines). Therefore, it becomes clear that the value of the polarization that has time to recover will be different for different gate voltage ranges at the same sweeping rate dV_g/dt, because the time required to reach different voltage values ($-2V$, $-4V$, $-6V$, $-8V$) will be different, and the corresponding polarization value that will have time to recover will be higher for a higher gate voltage V_g.

3.2.2. Impact of the ferroelectric substrate on the graphene carriers for low gate voltages

$Pb(Zr_xTi_{1-x})O_3$ (PZT) is a material of choice for GFETs [43, 49, 50], because its relative dielectric permittivity varies very sharply near the morphotropic phase boundary at $x = 0.52$. So, let us review the calculation results [16] of the graphene channel conductance on PZT substrate. Since the PZT response is not hysteretic for the electric fields smaller than the coercive field, E_c, (see Refs. [39, 42]), we will operate below within a relatively narrow gate voltage interval from –8V to +8V for which the linear response approximation $P(V_g)$ is valid. Therefore the further analysis should be similar to the one presented in 3.2.1, but the ferroelectric substrate permittivity value is much higher than unity.

Figure 3.2, *b* shows the carrier concentration in graphene calculated for different dipoles' relaxation times τ. The graphene channel on PZT substrate possesses the hole conductivity at $V_g = 0$ similarly to the case of SiO_2 substrate. For positive gate voltages, the holes concentration decreases and finally reaches the electroneutrality point, where the graphene valence band is completely occupied by electrons, and the conductance band is empty. The graphene channel conductivity switches to an electron one with a further increase of the gate voltage.

Figure 3.2, *d* presents the dependence of the carriers' concentration in the graphene channel on PZT substrate vs. the gate voltage calculated for its different amplitude $V_g^{\max}$. As anticipated, these dependences show the antihysteresis behavior and are qualitatively similar to those for graphene on SiO_2 substrate.

3.2.3. Impact of the ferroelectric substrate on the graphene carriers for high gate voltages

Figure 3.3 presents the carrier concentration in the graphene channel on the ideal ferroelectric substrate, $n(V_g)$, as a function of the gate voltage at room temperature. Figure 3.3 shows a pronounced hysteresis in the $n(V_g)$ dependence corresponding to the ferroelectric polarization reversal induced by a change of the gate voltage polarity from the maximal negative value $-V_g^{\max}$ to the positive one $+V_g^{\max}$. In contrast to the previous case (shown in Fig. 3.2), the hysteresis in Fig. 3.3 is caused by two different stable ferroelectric polarization states and can be used for nonvolatile memory cells [49, 50]. However, the corresponding switching times are comparative with the times of the ferroelectric domains reversal imposing strict limitations on the operating frequency (10^4–10^6) Hz for thick ferroelectric slabs. However, these times can be several orders of magnitude smaller (about 10^{-9} s) for thin ferroelectric films of thickness less than 100 nm [45].

Now, let us consider the case of gate doping by taking surface dipoles into account. In the case $P_s \neq 0, P_f \neq 0, n_T = 0$, two rival mechanisms of doping coexist. The first one originates from ferroelectric dipoles, and the second one steams from absorbed surface dipoles. Figure 3.4 presents the dependence of the carriers' concentration in the graphene channel on PZT ferroelectric substrate calculated for different rates of gate voltage sweeps (*a*–*b*). As one can see from Fig. 3.4, the existence of two rival channels of graphene doping modifies the form of hysteresis loops presented in the previous figures. As could be expected, the effect of absorbed surface molecules is es-

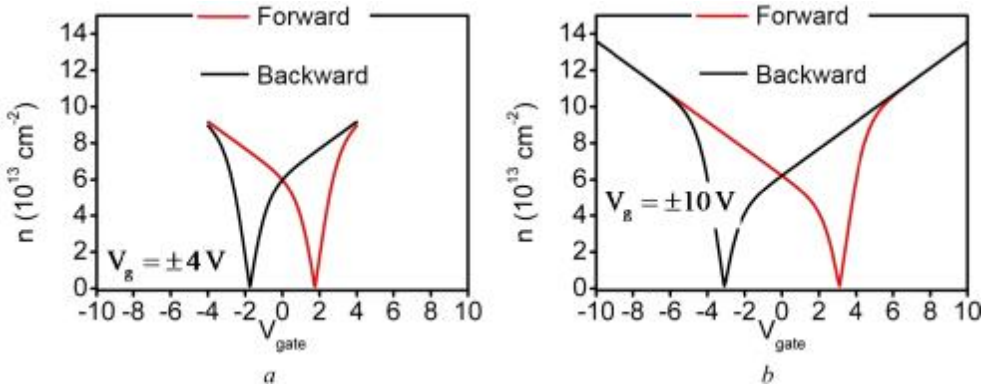

Fig. 3.3. The dependence of the carrier concentration in the graphene channel on the ideal ferroelectric substrate vs. the gate voltage calculated for different amplitudes of the gate voltage switching $V_g^{max} = \pm 4$ V (*a*) and $V_g^{max} = \pm 10$ V (*b*). Reproduced from [A.I. Kurchak, A.N. Morozovska, M.V. Strikha. *J. Appl. Phys.* **122**, 044504 (2017)], with the permission of AIP Publishing

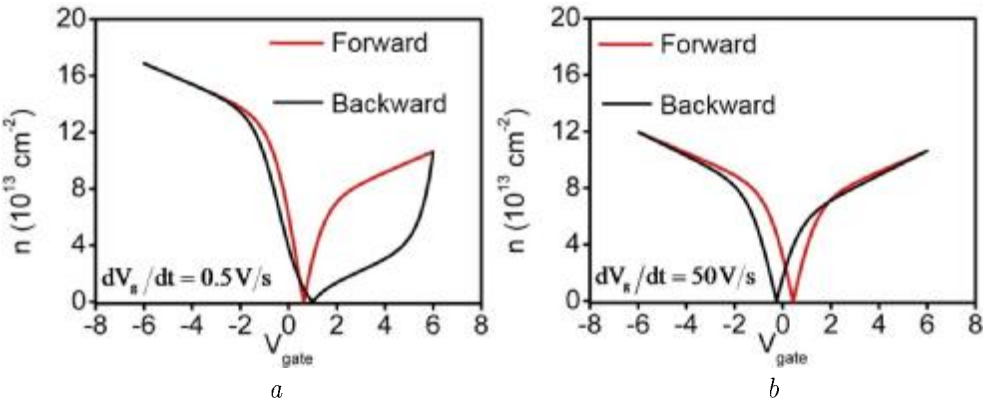

Fig. 3.4. The dependence of the carriers concentration in the graphene channel with surface absorbed dipoles on a real ferroelectric substrate on the gate voltage for different rates of gate voltage sweeps, $dV_g/dt = \pm 0.5$ V/s (*a*) and $dV_g/dt = \pm 50$ V/s (*b*). Reproduced from [A.I. Kurchak, A.N. Morozovska, M.V. Strikha. *J. Appl. Phys.* **122**, 044504 (2017)], with the permission of AIP Publishing)

sential at slow gate voltage sweeps, and the so-called antihysteresis occurs (Fig. 3.4, *a*). With the increase of dV_g/dt, the antihysteresis vanishes, and, finally, it transfers into the ferroelectric "direct hysteresis" with the increase of the distance between the electroneutrality points up to its final saturation (Fig. 3.4, *b*).

3.2.4. Comparison with experiment

To compare with realistic experiments, let us consider two rival mechanisms, which control the carriers concentration in graphene, the first one originating from ferroelectric dipoles and the second one steaming from absorbed surface dipoles. Figure 3.5 presents experimental [51] and theoretical results for the electroneutrality point positions as functions of the gate voltage sweeping rate for GFET with grapene sheet on the 140-nm $PbZr_{0.2}Ti_{0.8}O_3$/60-nm $SrRuO_3$/$SrTiO_3$ (001) heterostructure. Figure 3.5 the calculated values are in a reasonable agreement with experimental data [51]. The discrepancy between the theoretical and experimental dependences can be caused by the interface states between graphene and ferroelectric, as well as by the chemical doping of graphene during its fabrication.

We analyzed the origin of the hysteretic form of the graphene conductivity dependence on the gate voltage for graphene placed on different substrates. It was demonstrated that the increase of the gate voltage

sweeping rate dV_g/dt leads to the disappearance of a hysteresis for GFET on dielectric or ferroelectric substrates for the gate voltages less than the coercive one, $V_g < V_c$. The increase of the gate voltage rate causes the transition from antihysteresis to ferroelectric hysteresis. These results are in qualitative and quantitative agreement with the experimental data [51].

Note that the results of Ref. [52] have been obtained using several approximations and simplifications, which do not account for the specific physical nature of the binding to the graphene surface, the possible relaxation time spectrum, and the dependence of the carriers trapping by surface states on the gate voltage switching frequency in reality. The understanding of the effects is possible on the base of the clear vision of the physical mechanism of trapping and requires further studies.

In work [53], the hysteresis phenomenon in one- and multilayered graphene obtained using the method of chemical deposition from the vapor phase onto SiO_2 substrate was studied. The gate voltage was varied in the interval from 80 to +80 V, and the rate of its variation was changed considerably. Figure 3.6 schematically illustrates the dependences of the graphene channel conductivity on the voltage at the electrolytic gate (the aqueous solution of KCl was used as an electrolyte) for different voltage sweep rates. If the rate of voltage sweep decreases, the distance between the electroneutrality points also decreases, until they practically merge together at a rate of 0.0625 V/s. One can see that, at even lower rates, the "inverse" mechanism of hysteresis dominates. Such a behavior is in perfect agreement with the predictions made in the previous section of this work.

In Figure 3.7, the dependence of the "memory window" (the distance between the electroneutrality points, on the time interval needed for the system to return back from the switching point to the electroneutrality one is depicted by symbols. Here, we used the experimental data of work [53]. The curve shows the approximation of experimental data by the proposed model.

It is evident from Fig. 3.7 that a reduction of the "memory window," as the time interval of the surface dipole relaxation increases, is described well by the exponential dependence. It is worth to note that, owing to a strong coupling between the negative poles of dipoles with the graphene surface (see, e.g., work [54]), the time τ that is included into this dependence

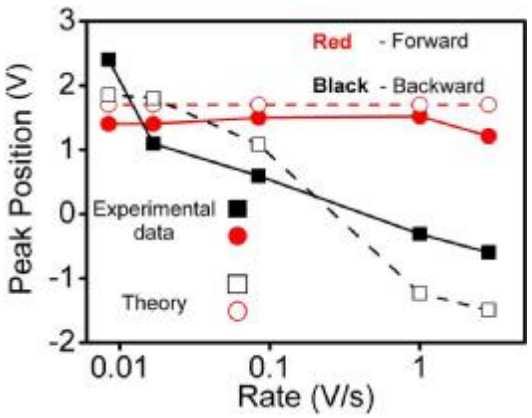

Fig. 3.5. Experimental [51] and theoretical values of electroneutrality point positions as function of the gate voltage sweeping rate for GFET on PZT ferroelectric substrate Reproduced from [A.I. Kurchak, A.N. Morozovska, M.V. Strikha. *J. Appl. Phys.* **122**, 044504 (2017)], with the permission of AIP Publishing

exceeds, by many orders of magnitude, the relaxation times that are characteristic of the polarization induced by free dipoles and described by a formula of the Langevin type. At the same time, the relaxation time for the concentration of charge carriers captured by the interface states is much longer. It equals hours at room temperature and tens of days at the nitrogen one [8]. Therefore, on the exponential time scale of work [53], this concentration can be regarded as dependent only on the gate voltage change.

We also examined the dependence of the graphene channel conductivity on the voltage at the standard Si gate at various sweep rates for this voltage both at high temperatures, when the adsorbed water molecules form a water layer, and at temperatures below the water freezing point, when the covering layer is ice. The chemical nature of those molecules is identical, but the mobility is different, namely, it is substantially higher in the fluid and lower in the crystal. This difference explains a discrepancy between the corresponding experimental dependences. In particular, in the case of ice, the direct hysteresis took place at high rates of voltage variation, and the inverse one at low rates. At the same time, in the case of water where the time of spontaneous restoration of a polarization is very short owing to a high mobility of dipoles, the inverse hysteresis was observed at any rate of voltage variation among those that were used in the experiment (see Fig. 3.8).

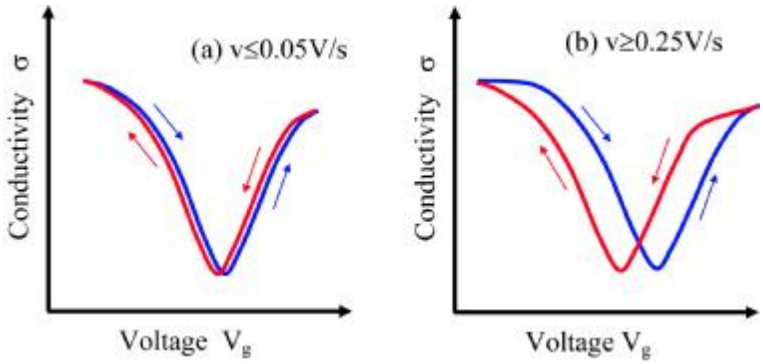

Fig. 3.6. Schematic plots of the dependences of the graphene channel conductivity on the voltage at the upper electrolytic gate V_g for various rates v of this voltage sweep (according to the experimental data of work [53])

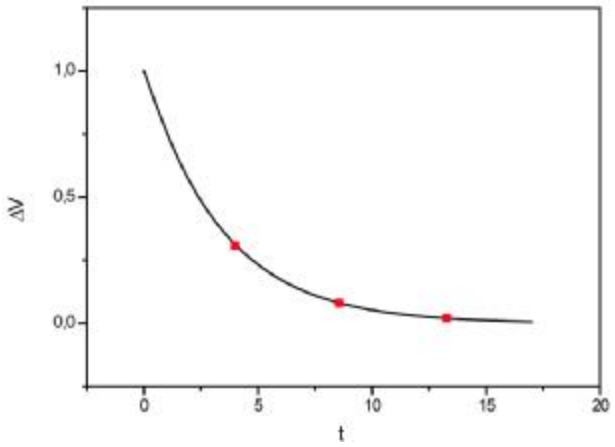

Fig. 3.7. Dependence of the "memory window" (in volt units) on the time needed for the system to return back from the switching point to the electroneutrality one (in seconds): experimental data of work [53] (symbols) and theory [42] (solid curve)

The results of comparison between the experimental data and the theoretical dependences, which was done in the previous section, testify that the model proposed in this work can describe the hysteresis phenomenon in the dependence of the conductivity in graphene channels created on the substrates of various origins on the gate voltage. The model provides a comprehension, on the quantitative level, of parameters inherent to the interface states and the polarization of an adsorbate bound with the free graphene surface and predicts an opportunity to distinguish between two hysteresis types, direct and inverse ones.

4. Dynamics of *p–n* Junctions in Graphene Channel Induced by the Motion of Ferroelectric Domain Walls

4.1. Theoretical formalism

In Section II, we considered the case of the fixed FDW. However, FDWs can move generally under external effects, which need a special examination. The review of theoretical works is based on Ref. [17]. The typical geometry of the GFET with a 2D-graphene layer (channel)-on-ferroelectric film with a 180-degree FDW is shown in Fig. 4.1, *a*. Top gate is deposited on the oxide layer, and the graphene sheet is separated from the ferroelectric film by an ultra-thin paraelectric dead layer originated due to several reasons, such as the incomplete polarization screening at the surface and the imperfect deposition process of graphene on the ferroelectric. There are different types of such layers treated as ultrathin and located under the surface of a ferroelectric substrate, where the spontaneous polarization is absent (or negligibly small) due to the surface contamination, zero extrapolation length, and/or strong depolarization field [55, 56]. A periodic voltage applied to the top gate can induce the motion of FDWs in the ferroelectric substrate.

The schematic of a pnJ created in the graphene channel by domain walls moving in a ferroelectric substrate is shown in Fig. 4.1, *b*. Since the lateral dimension of a ferroelectric film L_{FE} is typically much higher than the graphene channel length L, the odd, even, or fractional number of domain walls can pass along the channel during the period of the gate

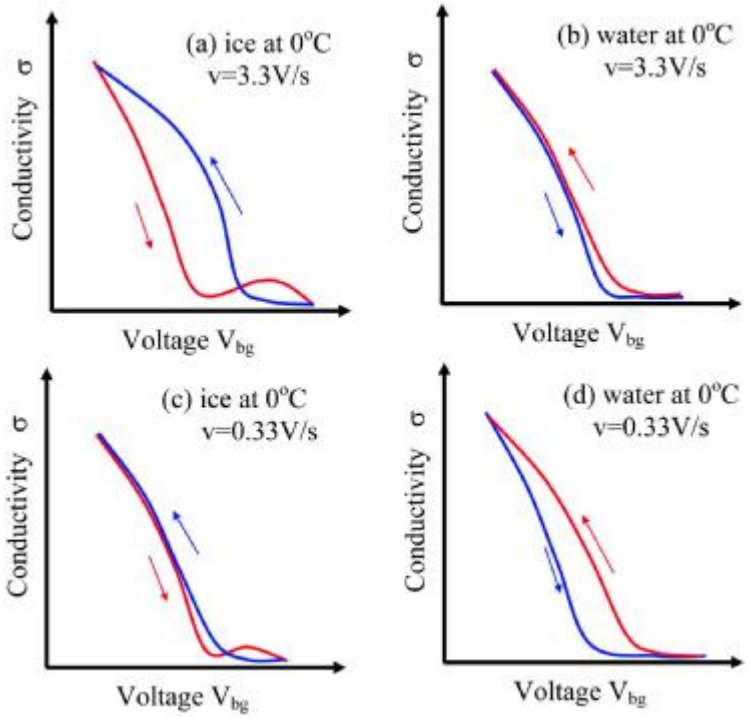

Fig. 3.8. Schematic plots of the dependences of the graphene channel conductivity on the gate voltage V_{bg} at various rates v of sweep of this voltage and at temperatures above (the adsorbate is water) and below (the adsorbate is ice) the freezing point (according to the experimental data of work [53])

voltage depending on the interrelation between the graphene channel length L and the period T_{FE} of the domain structure in a ferroelectric film.

A single-layer graphene is regarded as an infinitely thin sheet with two-dimensional (2D) electron density of electrons and holes states,

$$g_n(\varepsilon) = g_p(\varepsilon) = 2\varepsilon/\left(\pi\hbar^2 v_{\mathrm{F}}^2\right)$$

(see e.g. [3, 40]). Hence, the 2D concentrations of electrons in the conductance band and holes in the valence band of graphene are

$$n_{2\mathrm{D}}(\varphi) = \int_0^\infty d\varepsilon g_n(\varepsilon) f(\varepsilon - E_{\mathrm{F}} - e\varphi)$$

and

$$p_{2\mathrm{D}}(\varphi) = \int_0^\infty d\varepsilon g_p(\varepsilon) f(\varepsilon + E_{\mathrm{F}} + e\varphi),$$

respectively, E_{F} is a Fermi energy level. The graphene charge density is equal to

$$\sigma_G(\psi) = e\left(p_{2\mathrm{D}}(\psi) - n_{2\mathrm{D}}(\psi)\right),$$

where

$$\psi = \frac{e\varphi + E_{\mathrm{F}}}{k_{\mathrm{B}}T}.$$

The dependence of the 2D charge density of graphene on the dimensionless variable ψ is shown in Fig. 4.1, *c*.

The equations of state $\mathbf{D} = \varepsilon_0\varepsilon_{\mathrm{O}}\mathbf{E}$ and $\mathbf{D} = \varepsilon_0\varepsilon_{\mathrm{DL}}\mathbf{E}$ relate the electrical displacement $\mathbf{D}$ and electric field $\mathbf{E}$ in the oxide dielectric and ultrathin dead layers of thicknesses h_{O} and h_{DL}, respectively, ε_0 is a universal dielectric constant. The relative dielectric permittivity of the dead layer $\varepsilon_{\mathrm{DL}}$ is rather high $\sim 10^2$ [57]. The potential φ_{DL} satisfies Laplace's equation inside the dead layer. Note that the problem of the dielectric permittivity of a 2D-graphene layer is still under debate (see, e.g., [58]).

A ferroelectric film has thickness l and ferroelectric polarization P_3^{f} directed along its polar axis z with 180-degree domain wall – surface junctions [see Fig. 4.1]. The polarization z-component is

$$P_3(\mathbf{r}, E_3) = P_3^{\mathrm{f}}(\mathbf{r}, E_3) + \varepsilon_0\left(\varepsilon_{33}^b - 1\right)E_3,$$

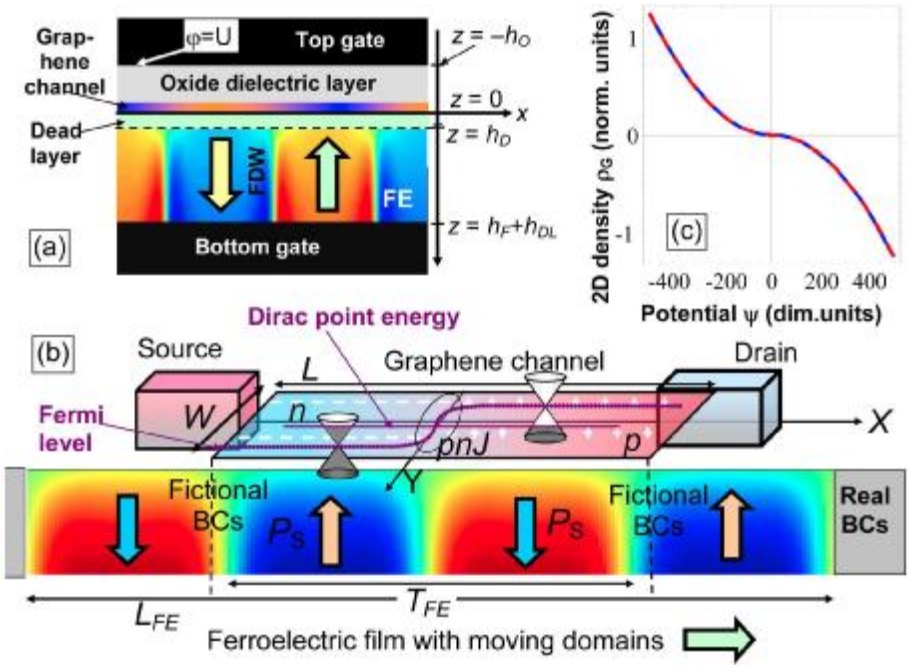

Fig. 4.1. Schematics of the 180°-ferroelectric domain walls (FDWs) in the "top gate - oxide dielectric layer – graphene channel – paraelectric dead layer – ferroelectric film – bottom gate" heterostructure (*a*). The ferroelectric substrate is in a perfect electric contact with the bottom gate electrode. Schematics of the pnJ induced in the graphene channel by domain walls moving in the ferroelectric substrate (*b*). Dependence of the 2D charge density of graphene on the dimensionless variable $\psi = \frac{e\varphi + E_F}{k_B T}$ (*c*). Reprinted from [A.I. Kurchak, *et al. Phys. Rev. Appl.* **8**, 024027 (2017)], with the permission of APS Publishing for the authors artwork

where the so-called relative "background" permittivity ε_{ij}^b is introduced [55]. The values of ε_{ij}^b are not related to a soft ferroelectric mode and limited by the linear dielectric response of the lattice. So, for the most of ferroelectrics perovskites, they are within the range (4–7) (see Ref. [59] for its determination and references therein). The spatial distribution of the ferroelectric polarization $P_3(x, y, z)$ is determined from the time-dependent LGD type Euler–Lagrange equation

$$\Gamma \frac{\partial P_3}{\partial t} + aP_3 + bP_3^3 + cP_3^5 - g\Delta P_3 = E_3. \qquad (4.1)$$

Γ is the Landau–Khalatnikov relaxation coefficient [60], g is a gradient coefficient, and Δ stands for the 3D-Laplace operator. The constants $a = = \alpha_T (T - T_C)$, b, and c are coefficients of the LGD potential expansion in the polarization powers (also called linear and nonlinear dielectric stiffness coefficients). The corresponding boundary conditions are of the third kind [61] with the extrapolation lengths $\Lambda_\pm$ [62].

For the problem geometry shown in Fig. 4.1, the system of electrostatic equations acquires the form listed in Ref. [17]. The boundary conditions for the system are fixed potentials at the top ($z = -h_O$) and bottom ($z = h_{DL} + h_F \approx h_F$) gate electrodes; the continuity of the electric potential at the graphene layer ($z = = 0$), and the equivalence of the difference of the electric displacement normal components

$$D_3^O = \varepsilon_0 \varepsilon_O E_3$$

and

$$D_3^{DL} = \varepsilon_0 \varepsilon_{DL} E_3,$$

to the surface charges in graphene

$$\sigma_G(x, y);$$

and the continuity of the displacement normal components

$$D_3^f = \varepsilon_0 \varepsilon_{33}^b E_3 + P_3^f$$

and

$$D_3^{DL} = \varepsilon_0 \varepsilon_{DL} E_3,$$

at the dead layer/ferroelectric interface. The gate voltage is periodic with a period T_g,

$$U(t) = U_{\max} \sin(2\pi t/T_g).$$

To generate moving domains, the ferroelectric film thickness should be above the critical thickness $l_{\rm cr}$ of the size-induced phase transition into a paraelectric phase. In this case, $l_{\rm cr}$ depends on the dielectric and dead layer thicknesses [63–65]. The domains appear above the critical thickness, since they minimize the depolarization field energy in the gap and dielectric layer [66].

Since the lateral dimension of a ferroelectric film $L_{\rm FE}$ is typically much higher than the graphene channel length L, the *odd*, *even*, or *not fractional* number of domain walls can pass along the channel during the period of the gate voltage T_g depending on the interrelation between the graphene channel length L and the period $T_{\rm FE}$ of the domain structure in a ferroelectric film (see Ref. [17]). The realistic situations can be modeled by a *periodic, mixed, or antiperiodic* boundary conditions (BCs) imposed on the polarization component P_3, its derivative $\frac{\partial P_3}{\partial x}$, electric potential φ_f, and its derivative $\frac{\partial \varphi_f}{\partial x}$ at the lateral boundaries $x = \pm L/2$ [17].

Using the results in [15, 17] for the *even* number ($2k$) of walls between the source and drain electrodes of the graphene channel, its conductances $G_+^{\rm total}$ and $G_-^{\rm total}$ are equal for both polarities of the gate voltage $\frac{G_+^{\rm total}}{G_-^{\rm total}} = 1$, because, for each polarity, there are k p–n junctions with conductance given by Eq. (8) of [15] and k p–n junctions with conductance given by Eq. (10) of [15]. For the *odd* number of walls, $2k$+1, Eq. (14) of Ref. [15] can be modified as

$$\frac{G_+^{\rm total}}{G_-^{\rm total}} = \frac{\beta(L+\lambda) + \lambda k(1+\beta)}{\beta(L+\lambda) + \lambda k(1+\beta) + \lambda}, \qquad (4.2)$$

where the factor

$$\beta = \sqrt{\frac{\pi\alpha c}{4\varepsilon_{33}^{\rm f} v_{\rm F}}}$$

is proportional to the squire root of the fine structure constant α, light velocity in vacuum c, and inversely proportional to the relative ferroelectric permittivity $\varepsilon_{33}^{\rm f}$ and the Fermi velocity of electrons in graphene $v_{\rm F}$. The electron mean free path λ is typically essentially smaller than the channel length L.

For a pronounced diffusion regime of the current, $\beta L \gg \gg \lambda$, as well as for the great number of walls, $k \gg k_{\rm cr}$, where

$$k_{\rm cr} = 1 + \frac{\beta L}{(1+\beta)\lambda},$$

the conductance of the graphene channel is given by the expression [3, 40]

$$G = \frac{\lambda(n_{\rm 2D})}{L} \frac{2e^2}{\hbar\pi^{3/2}} W\sqrt{n_{\rm 2D}},$$

being proportional to the product of the graphene channel width W by the squire root of the 2D charge concentration $n_{\rm 2D}$. The mean free path $\lambda(n_{\rm 2D}) \sim \sqrt{n_{\rm 2D}}$ for the scattering at ionized centers in the substrate and in the temperature range far from Curie temperature [3].

4.2. Analyses of ferroelectric domains and p–n junctions correlated dynamics

Below, we present the results of numerical modeling of the considered problem. Parameters used in the calculations are listed in Table I in Ref. [17]. The polarization component in the ferroelectric film P_3, variation of the 2D-concentration of free carriers in the graphene channel $\Delta n_G = (p_{\rm 2D} - n_{\rm 2D})$, and the effective conductance ratio

$$\Delta\eta(U_{\max}) = \frac{\Delta n_G(+U_{\max})}{\Delta n_G(-U_{\max})}$$

were calculated in dependence on the periodic gate voltage

$$U(t) = U_{\max} \sin(2\pi t/T_g).$$

The hysteresis loops of the average polarization $P_3(U)$ and the concentration variation $\Delta n_G(U)$ are shown in Fig. 4.2. At relatively low voltages ($\leqslant$2 V), the polarization and concentration loops have quasielliptic shape [see black curves in Fig. 4.2, *a*–*d*]. This happens because the film state is polydomain, and the domain walls are moved by the electric field with the gate voltage changing from $-U_{\max}$ to $+U_{\max}$. With the increase of the gate voltage amplitude $U_{\max}$ to (5–10) V, the domain walls start to collide, and the domains with opposite polarization orientation almost "annihilate" for definite periodic moments of time t, and then the polar state of the film with some degree

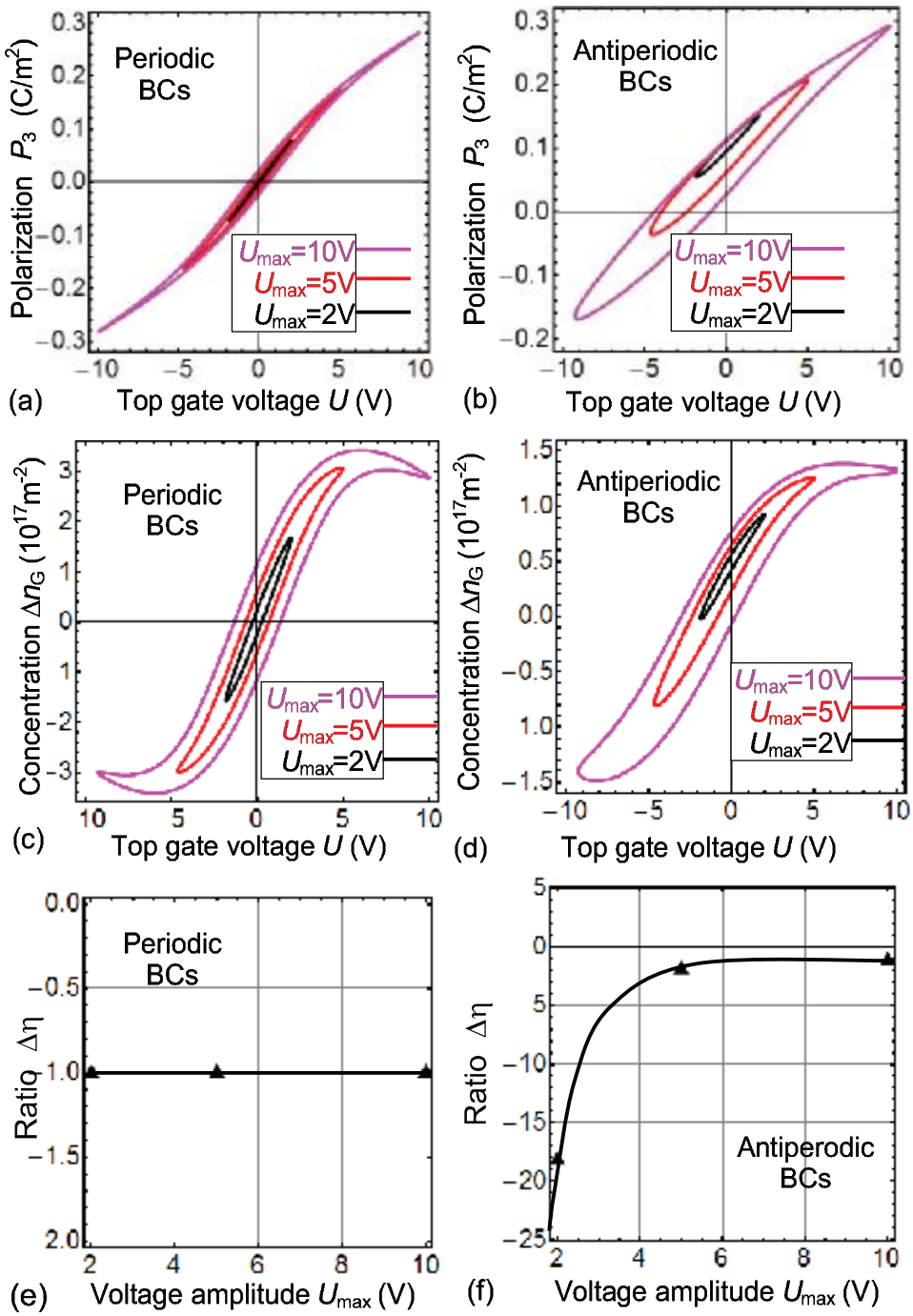

Fig. 4.2. Hysteresis loops of the ferroelectric polarization $P_3(U)$ (*a*, *b*), carriers concentration variation in a graphene channel $\Delta n_G(U)$ (*c*, *d*), and the conductance ratio $\Delta\eta(U_{\max})$ (*e*, *f*) calculated for periodic (*a*, *c*, *e*) and antiperiodic (*b*, *d*, *f*) boundary conditions (BCs). Black, red, and magenta loops correspond to the different amplitudes of the gate voltage $U_{\max} = (2, 5, 10)$ V and the gate voltage period $T_g = 10^3$ s. Adapted from [A.I. Kurchak, *et al. Phys. Rev. Appl.* **8**, 024027 (2017)] with the permission of APS Publishing for the authors artwork

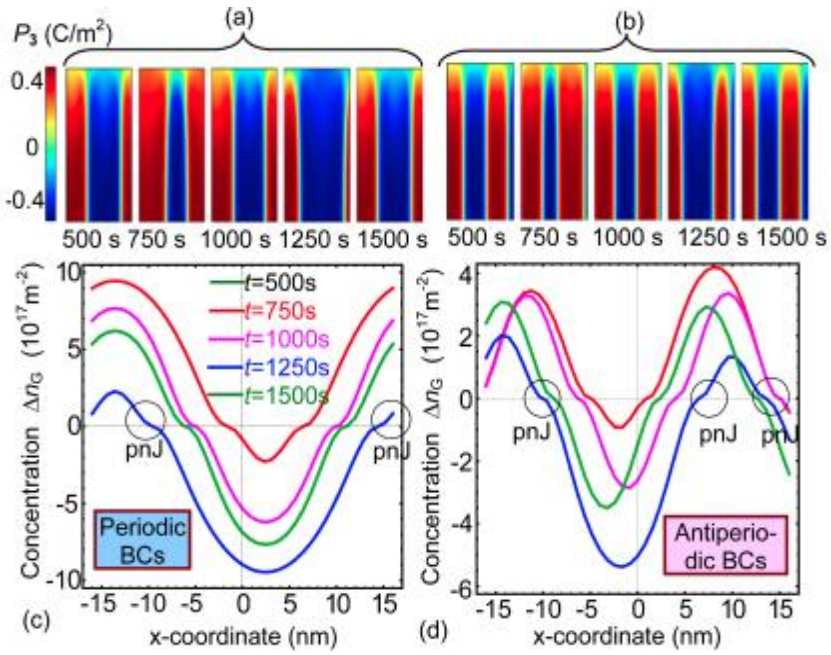

Fig. 4.3. Spatial distribution of the polarization component P_3 in a ferroelectric film calculated at certain times over a period, 500, 750, 1000, 1250, and 1500 s (specified in the plots) for the periodic (*a*) and antiperiodic (*b*) BCs. The 2D-concentration of the free charge $\Delta n_G(x,t)$ calculated along the graphene channel at certain times over a period, 500, 750, 1000, 1250 and 1500 s (specified in the plots) for the periodic (*c*) and antiperiodic (*d*) BCs. Gate voltage amplitude $U_{\max} = 5$ V and period $T_g = 10^3$ s. Other parameters are the same as in Fig. 3.2. The transient process that vanishes enough rapidly is not shown (so that, we show the plots from times $t \geqslant 500$ s). Adapted from [A.I. Kurchak, *et al. Phys. Rev. Appl.* **8**, 024027 (2017)] with the permission of APS Publishing for the authors artwork

of unipolarity partially restores [see red and magenta curves in Fig. 4.2, *a*–*d*]. The loops asymmetry and rectification ratio is defined by the symmetry of the BCs for the polarization and the electric potential at the lateral surfaces $x = \pm L/2$.

Completely symmetric loops of polarization $P_3(U)$ and concentration $\Delta n_G(U)$ variation correspond to the periodic BCs [Figs. 4.2, *a* and 4.2, *c*]. The rectification effect is absent in the case of periodic BCs, since the effective ratio $\Delta\eta(U_{\max}) \equiv -1$ for all $U_{\max}$ [see Fig. 4.2, *e*], because the even number of domain walls is moving in the ferroelectric substrate at any time. Characteristic distributions of the polarization component P_3 and free charge concentration along the graphene channel are shown in Figs. 4.3, *a* and 4.3, *c*, respectively. Two *p*–*n* junctions are induced by two moving domain walls at certain times over one period.

The antiperiodic BCs lead to asymmetric loops of polarization $P_3(U)$ and concentration $\Delta n_G(U)$ [Figs. 4.2, *b* and 4.2, *d*]. The vertical asymmetry and horizontal shift of the $P_3(U)$ loop are much stronger than the asymmetry of the $\Delta n_G(U)$ loop, because the polarization acts on the charge indirectly via the depolarization field. The asymmetry of $P_3(U)$ and $\Delta n_G(U)$ becomes weaker, as the maximal voltage increases [compare different loops in Figs. 4.2, *c* and 4.2, *f*]. The rectification effect is evident for low and moderate voltages, since the effective ratio $\Delta\eta(U_{\max}) \ll 1$ for $1 < U_{\max} < 4$, and the ratio saturates, $\Delta\eta(U_{\max}) \to -1$, for higher voltages [see Fig. 4.2, *f*], because the odd number of domain walls are moving in the ferroelectric film for most of the time. Characteristic distributions of the polarization and graphene charge are shown in Figs. 4.3, *b* and 4.3, *d*, respectively. Three *p*–*n* junctions are induced by the three moving domain walls over one period.

4.3. Extrinsic size effect

Note that the conductivity of the graphene channel (that is proportional to the total carrier concentration

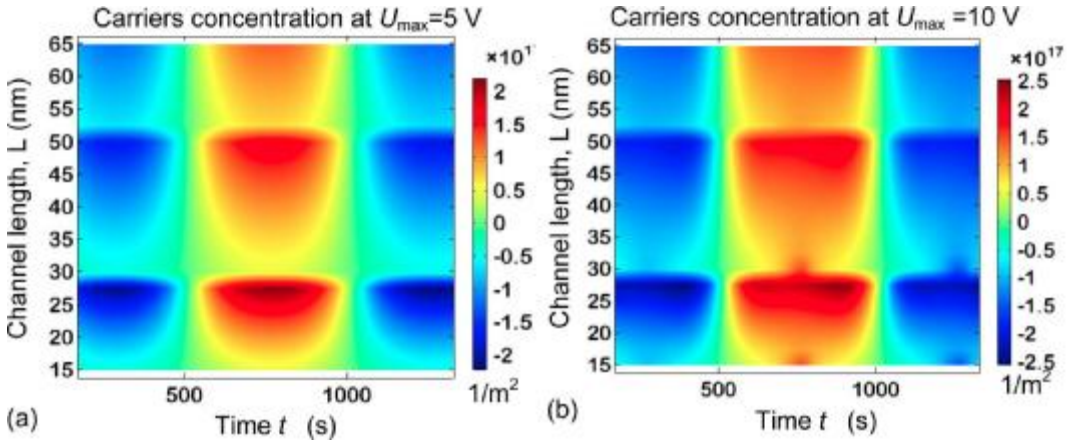

Fig. 4.4. Dependence of the graphene channel conductivity on its length and time calculated for the periodic BCs at $U_{\max} = 5$ V (*a*) and $U_{\max} = 10$ V (*b*). Adapted from [A.I. Kurchak, *et al. Phys. Rev. Appl.* **8**, 024027 (2017)] with the permission of APS Publishing for the authors artwork

variation $\Delta n_G(L,t)$) depends on its length L [see the contour map of the average concentration variation $\Delta n_G(L,t)$ in the coordinates "channel length L – time t" in Fig. 4.4]. The phenomenon we called "extrinsic size effect" [15] consists in a quasiperiodic modulation of the conductivity amplitude with the channel length for periodic BCs. In thid case, the modulation extremes are the most pronounced for L around 27.5 nm (the first maxima and minima depending on the time moment) and 50 nm (the second maxima and minima) at the parameters listed in Ref. [15]. The modulation becomes less pronounced, as L increases [compare the contrast for the modulation maxima and minima at $L = 27.5$ nm and 50 nm]. The distance ΔL between the maxima is voltage-independent and slightly increases with L. We expect that the extrinsic size effect will disappear for long channels, whose length is much longer than the intrinsic period of the domain structure in a ferroelectric substrate.

5. Graphene Separation and Stretching Induced by the Piezoelectric Effect of Ferroelectric Domains

p–n junctions in graphene on ferroelectric substrates have been actively studied, but the impact of the piezoelectric effect in a ferroelectric substrate with ferroelectric domain walls (FDWs) on graphene characteristics was considered only recently. Namely, as it has been shown in Ref. [18], the elastic strain can significantly affect the graphene conductance via the *stretching* of its surface and *separation* of graphene areas at the steps between elongated and contracted domains. The theoretical formalism presented in this section is based on Ref. [18].

The idea is that ferroelectric domain stripes with opposite spontaneous polarizations elongate or contract depending on the polarity of a voltage applied to the substrate due to the piezoeffect. If the voltage is applied to a gate of the GFeFET with FDW, one domain elongates and another one contracts depending on the voltage polarity [see Fig. 5.1]. The surface displacement can be significant for ferroelectrics with high piezoelectric coefficients such as $PbZr_{0.5}Ti_{0.5}O_3$ (PZT), whose piezoelectric coefficients can reach (0.3–1) nm/V depending on the film thickness and temperature [67]. The corresponding piezoelectric surface displacement step h is about (0.5–1) nm for the gate voltage ~(1–3) V. The thickness $d \leqslant 0.5$ nm of the physical gap between graphene and ferroelectric is determined by the van-der-Waals interaction. The density J of the binding energy for graphene on SiO_2 substrate is about 0.5 J/m^2 [68]. Because the graphene adhesion to SiO_2 should be the strongest one in comparison with other surfaces, it is natural to expect that J for graphene on PZT surface is smaller. The Young modulus Y of graphene is giant, 1 TPa, [69,70]. Under these conditions, the partially separated graphene region occurs at the step, when the normal component F_n of the elastic tension force F applied to a carbon atom exceeds the force F_b binding the atom with the surface [see the scheme of forces in Fig. 5.1, *b*. The separated

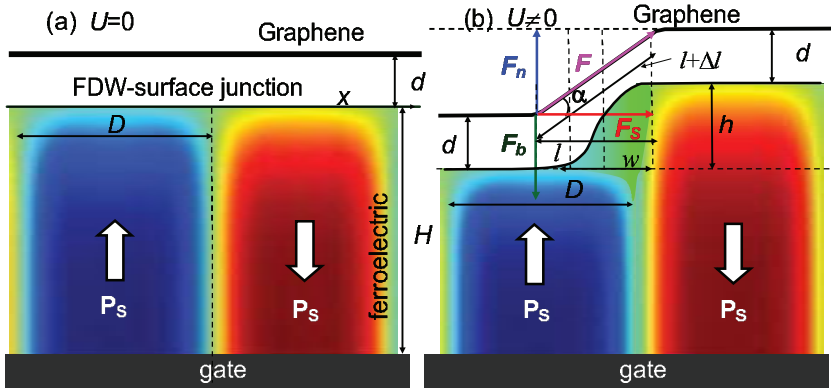

Fig. 5.1. Partial separation of graphene channel sections induced by the piezoelectric effect at the ferroelectric domain wall – surface junction. The separation is absent at the zero applied voltage $U = 0$ (*a*) and appears at a nonzero one $U \neq 0$ (*b*). F is the elastic tension force, F_n is its normal component, F_S is its lateral component and F_b is the binding force of a carbon atom to the surface. Adapted from [A.N. Morozovska, A.I. Kurchak, M.V. Strikha. *Phys. Rev. Appl.* **8**, 054004 (2017)] with the permission of APS Publishing for the authors artwork

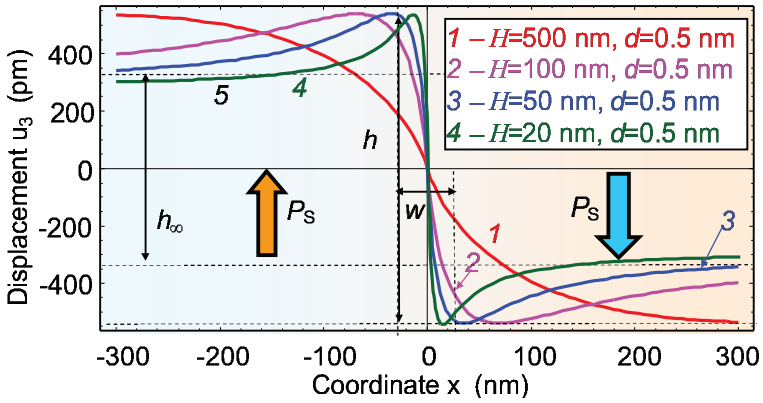

Fig. 5.2. Profiles of the ferroelectric surface displacement u_3 calculated at the gate voltage $U = 1$ V, thermodynamic piezoelectric coefficients $d_{33} \approx 10^3$ pm/V, $d_{31} \approx -450$ pm/V, and Poisson ratio $v = 0.3$ corresponding to PZT at room temperature. The values of ferroelectric film thickness H and distance d for curves *1–4* are indicated in the legend. Note that the vertical picometer scale is much smaller than the horizontal nanometer scale. Adapted from [A.N. Morozovska, A.I. Kurchak, M.V. Strikha. *Phys. Rev. Appl.* **8**, 054004 (2017)] with the permission of APS Publishing for the authors artwork

section with the length $l + \Delta l$ is "*suspended*" between the bounded sections.

5.1. Piezoelectric displacement of the ferroelectric substrate surface

An analytical expression for the vertical displacement $u_3(x)$ in a vicinity of the FDW-surface junction is derived in Ref. [18] within the framework of the decoupling approximation [71–75]. The displacement $u_3(x)$ takes the form [18]:

$$u_3(x) = -U\,[W_{33}(x)\,d_{33} + W_{31}(x)\,d_{31}]. \qquad (5.1)$$

U is the voltage between the top and bottom electrodes, i.e. the gate voltage; d_{33} and d_{31} are piezoelectric coefficients. The specific forms of $W_{33}(x)$ and $W_{31}(x)$ are given in Ref. [18].

Figure 5.2 shows the typical profiles of the PZT surface displacement calculated for the gate voltage $U = 1$ V and room temperature. Values of the PZT film thickness H are in the interval $H = (20\text{–}500)$ nm, and the separation $d = 0.5$ nm. One can see from the figure that the step originated at the FDW-surface junction is the widest for the smallest ratio d/H (curve *1*) and becomes essentially thinner, as the ratio

increases (curves *2–4*). As one can see, the maximal height h of the step changes in a nonmonotonic way, as d/H ratio increases, but the displacement difference far from the domain wall,

$$h_\infty = |u_3(x \to \infty) - u_3(x \to -\infty)|,$$

is the same for all curves and is given by the expression [18]:

$$h_\infty = 2|U|[d_{33} + (1+2\nu)d_{31}]. \quad (5.2)$$

The complete separation (i.e. exfoliation) of graphene caused by the piezoelectric effect is hardly possible in thick ferroelectric films with smooth profiles of the surface displacement corresponding to curve *1* in Fig. 5.2. The complete exfoliation becomes impossible, if the domain wall is a single one in a film; and so only the stretching of the graphene sheet is induced by the piezoelectric effect in this case. The partial separation or complete exfoliation of graphene can be favorable, when it contacts with relatively sharp ferroelectric surface profiles across the FDWs corresponding to curves *2–4* in Fig. 5.2.

5.2. Graphene separation, stretching, and exfoliation: impact on the conductance

The complete exfoliation becomes impossible, if the domain wall is a single one in a thick film; and so only the stretching of the graphene sheet is induced by the piezoelectric effect. The case of graphene stretching by the piezoelectric effect in a thick film is shown in Fig. 5.3, *a*. The scheme of the graphene partial separation or complete exfoliation caused by the piezoelectric effect in a thin film is shown in Fig. 5.3, *b*. The separated sections are suspended and fixed between the bounded graphene regions. The stretching of the suspended graphene regions can be strong enough in the case of its partial fixing by the ferroelectric surface [see curve *1* in Fig. 5.3, *b*], if the van-der-Waals forces can keep the graphene at the bottom of the cavities induced by the piezoelectric effect on the domain structure. The graphene stretching is almost absent in the case of its complete exfoliation from the ferroelectric surface due to the weakness of the van-der-Waals forces, and the graphene sheet is suspended above the bottoms of domains wells [see curve *2* in Fig. 5.3, *b*].

All cases, namely the stretching, partial separation, or complete exfoliation, can be realized in a real system depending on the binding energy J and distance d. The *ab initio* calculations are required to answer the question and all possible cases of graphene mechanical behavior can be realized for a given piezoelectric displacement of the ferroelectric film surface. Our calculations show that, depending on the ratios D/H and d/h, the situations with the graphene stretching and partial separation can be very different [compare Figs. 5.3, *a* and 5.3, *b*]. The length of the graphene section separated from the ferroelectric surface can be estimated for the sharp profile of the surface displacement. In this case, the graphene surface profile is approximated by dotted lines, as shown in Fig. 5.3, *b*. It is natural to expect that the graphene separation occurs right to the point, where the normal component F_n of the tangential force F and the binding force F_b are equal [see Fig. 5.3, *b*].

Taking into account that the normal component F_n of the tangential force F and the binding force F_b are equal [see Fig. 5.3, *b*], we derived the analytical expression for the minimal length l of a separated graphene region [18],

$$l = h\sqrt[3]{\frac{Yd}{2J}} > |U|(d_{33} + (1+2\nu)d_{31})\sqrt[3]{\frac{4Yd}{J}}. \quad (5.3)$$

The inequality in Eq. (5.3) originates from the inequality $h > h_\infty$ [see Fig. 5.2]. Estimates made from Eq. (5.3) give that the stretched section can reach tens of nm for the gate voltages $|U| \geqslant 3$ V, PZT parameters at room temperature, binding energies $J < 0.25$ J/m^2, and separation $d = 0.5$ nm.

The conductance of the graphene channel in the diffusion regime can change significantly, because electrons in the separated stretched section scatter on acoustic phonons [40]. The voltage dependence of the conductance $G(U)$ of the graphene channel of length L, when its part of length $l(U)$ is separated and another part of length $L - l(U)$ is bounded, obeys the Matthiessen rule [40]:

$$G(U) = W\left[\frac{L - l(U)}{\sigma_B} + \frac{l(U)}{\sigma_S}\right]^{-1}. \quad (5.4)$$

The separated length $l(U) = \chi|U|$, where the coefficient

$$\chi = (d_{33} + (1+2\nu)d_{31})\sqrt[3]{4Yd/J}$$

in accordance with Ref. [18].

The conductivity of the bounded section has the form [3]:

$$\sigma_B = \frac{2e^2}{\pi^{3/2}\hbar}\lambda_B\sqrt{n_{2D}}. \quad (5.5)$$

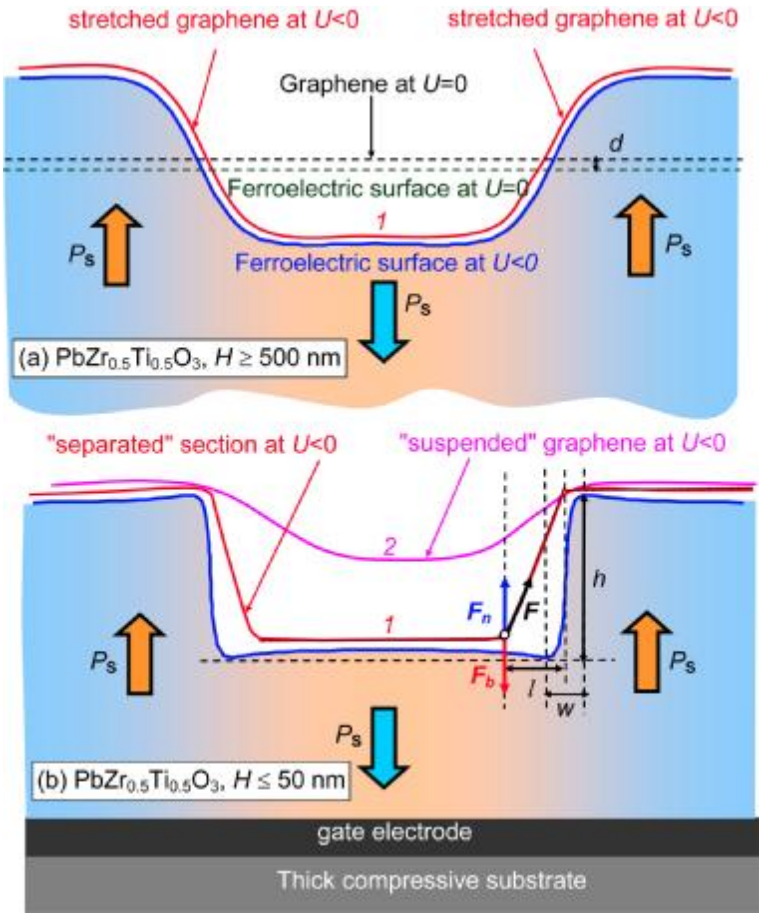

Fig. 5.3. Schematic profiles of the ferroelectric film and graphene surface displacements for $U = 0$ (dashed horizontal lines) and $U < 0$ (solid curves *1*, *2*). (*a*) Graphene stretching (without any separation) induced by the piezoelectric effect in thick films with smooth profile of the surface displacement across the FDWs (curve *1*). (*b*) Partial (curve *1*) and complete (curve *2*) separation of a graphene region induced by the piezoelectric effect in thin films with sharp profile of the surface displacement across the FDWs. Note that the vertical scale is much smaller than the horizontal one and $l \gg h$. Adapted from [A.N. Morozovska, A.I. Kurchak, M.V. Strikha. *Phys. Rev. Appl.* **8**, 054004 (2017)] with the permission of APS Publishing for the authors artwork

Here, e is the elementary charge, $\hbar$ is the Planck constant, $v_F = 10^6$ m/s is a characteristic electron velocity in graphene, λ_B is the mean free path in the bounded part of the graphene channel. The concentration of 2D electrons n_{2D} can be regarded as constant voltage-independent far from the FDWs, namely $n_{2D} \approx |P_S/e|$ [17, 18, 34]. Using that, in the most common case of electron scattering in the graphene channel at ionized impurities in a substrate,

$$\lambda_B\,[n_{2D}] = \xi\sqrt{n_{2D}},$$

where the proportionality coefficient ξ depends on the substrate material and graphene-ferroelectric interface chemistry, we obtain the following dependence from Eq. (5.5):

$$\sigma_B\,[n_{2D}] = \frac{2e^2\xi}{\pi^{3/2}\hbar} n_{2D} \approx 8.75 \times 10^{-5}\xi n_{2D}$$

(in Siemens). Taking into account that P_S value can be 10 times smaller for thin films than its bulk value, the concentration varies in the interval $n_{2D} \cong (0.3\text{–}3) \times 10^{18}$ m^{-2} depending on the film thickness, but should be regarded as a voltage- and coordinate-independent constant far from the FDW. Thus, elementary estimates give $\sigma_B \cong (0.15\text{–}15) \times 10^{-3}\Omega^{-1}$ for the reasonable intervals of $\lambda_B = (10\text{–}100)$ nm and $P_S = (0.05\text{–}0.5)$ C/m^2.

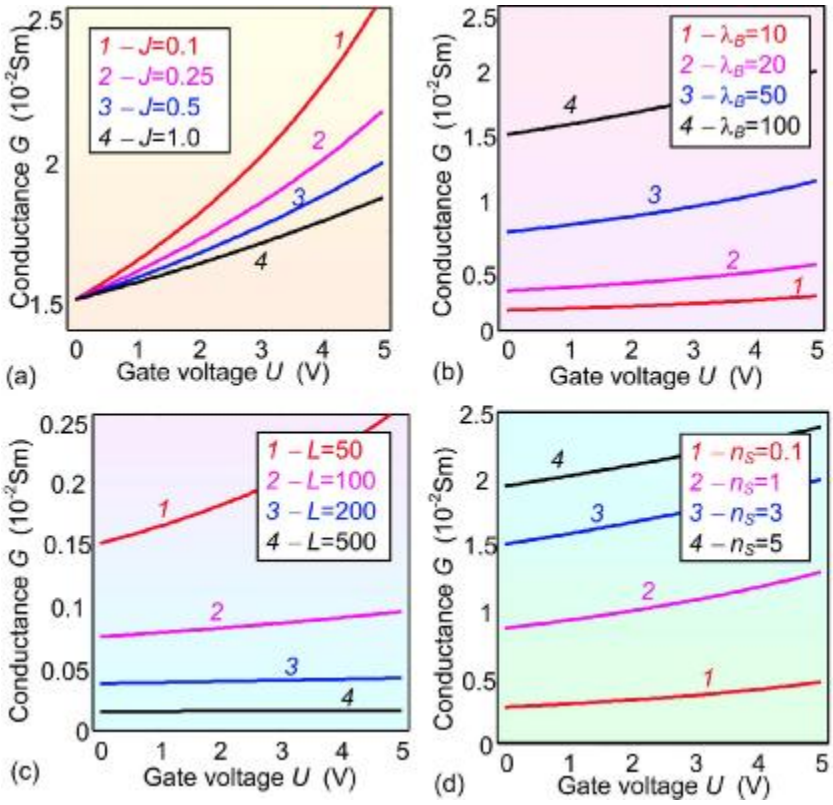

Fig. 5.4. Dependences of the conductance $G(U)$ on the gate voltage U calculated for several values (curves *1–4*) of the binding energy $J = 0.1$, 0.25, 0.5, and 1.0 J/m^2 (*a*); electron mean free path $\lambda_B = 10$, 20, 50, 100 nm (*b*); channel length $L = 50$, 100, 200, 500 nm (*c*); and concentration $n_S = (0.1, 1, 3, 5) \times 10^{18}$ m^{-2} (*d*). Piezoelectric coefficients $d_{33} \approx 10^3$ pm/V, $d_{31} \approx -450$ pm/V and Poisson's ratio $v = 0.3$ corresponds to $PbZr_{0.5}Ti_{0.5}O_3$, $n_S = 3 \times 10^{18}$ m^{-2}, $\lambda_B = 100$ nm, $L = 50$ nm, $W = 50$ nm, and separation $d = 0.5$ nm, graphene Young modulus $Y = 1$ TPa, binding energy $J = 0.5$ J/m^2. Reprinted from [A.N. Morozovska, A.I. Kurchak, M.V. Strikha. *Phys. Rev. Appl.* **8**, 054004 (2017)] with the permission of APS Publishing for the authors artwork

On the contrary, the main channel for the electron scattering in the separated stretched section of structurally perfect graphene is collisions with acoustic phonons. In this case, $\lambda_S(E) \sim 1/E$ [3]. This leads to the well-known paradox: conductivity σ_S doesn't depend on the 2D electron concentration in the graphene channel. Hence, for estimations the well-known upper limit for σ_S [3] can be used:

$$\sigma_S = \frac{4e^2\hbar\rho_m v_F^2 v_S^2}{\pi D_A^2 k_B T}. \qquad (5.6)$$

Here, $\rho_m \approx 7.6 \times 10^{-7}$ kg/m^2 is the 2D mass density of carriers in graphene, $v_S \approx 2.1 \times 10^4$ m/s is the sound velocity in graphene, Boltzmann constant $k_B = 1.38 \times 10^{-23}$ J/K; $D_A \approx 19$ eV is the acoustic deformation potential that describes the electron-phonon interaction. Expression (5.6) yields $\sigma_S \approx 3.4 \times 10^{-2}\Omega^{-1}$ at room temperature.

Figure 5.4 presents the conductance G calculated for different values of gate voltage U, binding energy J, electron mean free path λ_B, channel length L, and concentration n_S. The conductance increases with U; in this case, the increase is monotonic and faster than linear (i.e. "superlinear") at fixed other parameters. The increase is the most pronounced at small binding energies $J \leqslant 0.2$ J/m^2 [Fig. 5.4, *a*], long mean free paths $\lambda_B \geqslant 50$ nm [Fig. 5.4, *b*], small channel length $L \leqslant 100$ nm [Fig. 5.4, *c*], and relatively high concentrations $n_S \geqslant 10^{18}$ m^{-2} [Fig. 5.4, *d*].

The conductance increases with U; the increase is monotonic and faster than linear and mostly pronounced at small binding energies $J \leqslant 0.2$ J/m^2 [Fig. 5.4, *a*] and small channel lengths $L \leqslant 100$ nm

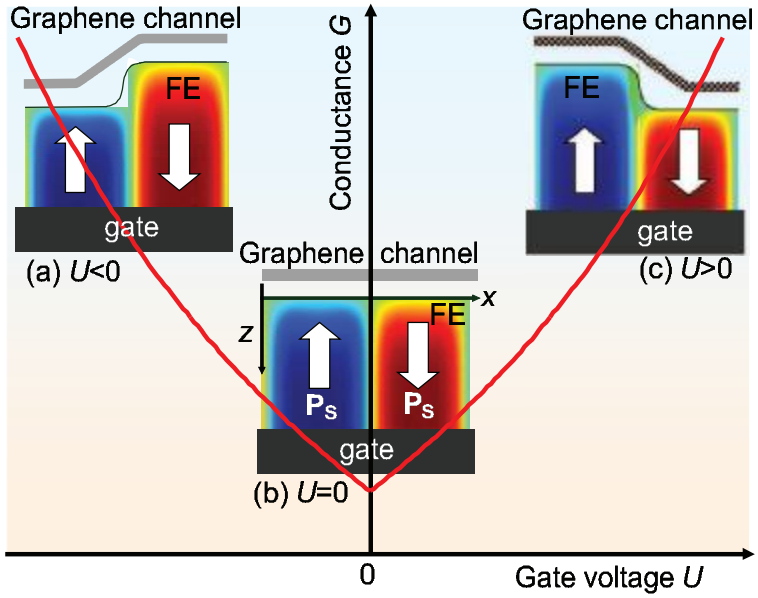

Fig. 5.5. Modulation of the graphene channel conductance by the piezoeffect in GFeFET. Main plot shows the schematic dependence of the channel conductance $G(U)$ on the gate voltage U. Insets (a) and (c) illustrate the vertical piezoelectric displacement of the ferroelectric surface at FDW that causes the partial separation of graphene sections induced by negative and positive gate voltages, respectively. The displacement and corresponding graphene separation are absent at $U = 0$ [Inset (b)]. Adapted from [A.N. Morozovska, A.I. Kurchak, M.V. Strikha. *Phys. Rev. Appl.* **8**, 054004 (2017)] with the permission of APS Publishing for the authors artwork

[Fig. 5.4, *c*]. The conductance ratio $G(U)/G(0)$ doesn't exceed 1.25 in the case of graphene partial separation [presented by the red curves] at realistic values of parameters. However, it can be significantly greater, if the domain stripe period D is much shorter than the channel length L. In this case, the length L is divided in two almost equal parts between the separated and bonded sections (i.e. $l \approx L/2$). If the p–n-junctions at FDW don't change the general conductance of the graphene channel significantly, the electron mean free passes $\lambda_B \ll D$, $\lambda_S \ll D$ and $\sigma_S \gg \sigma_B$, Eq. (5.4) yields $\frac{G(U)}{G(0)} \approx 2$. Note that the ratio $G(U)/G(0)$ can be significantly greater than 2, e.g., in the case of mostly suspended graphene ($l \approx L$) with $\sigma_S \gg \sigma_B$. However, the possibility of such a limiting case needs a special examination.

Figure 5.5 schematically illustrates the conductance $G(U)$ calculated from Eqs. (5.4)–(5.6). The predicted effect of conductance modulation can be very useful for the improvement and miniaturization of various electronic devices (such as advanced logic elements, memory cells, highly efficient hybrid electrical modulators and transducers of voltage-to-current type, and piezoresistive elements). We propose an alternative method of fabrication of suspended graphene areas based on the piezoeffect in a ferroelectric substrate. The method does not require any additional technological procedures like chemical etching or mechanical treating of the substrate surface.

Notably, the separated sections of the graphene channel induced by the piezoeffect can cause the physical effects, which are of interest for fundamental physics. First, the graphene channel conductance in the diffusion regime is changed significantly, because electrons in the stretched section scatter on acoustic phonons. Second, mechanic vibrations in the MHz range can be realized here [76]. Third, high pseudomagnetic fields were reported for stretched graphene [77].

6. Conclusions

Since GFETs on ferroelectric substrates are promising candidates for the novel nonvolatile ultra-fast ferroelectric memories (FRAM) [49], [50]], the theoretical description of the devices operation requires reliable knowledge about the ferroelectric response in a wide frequency range, as well as the nature of carrier trapping processes at a given frequency.

It has been shown that the contact between the domain wall and the ferroelectric surface creates a p–n junction in the graphene channel, so that the carrier concentration induced in graphene by uncompensated ferroelectric dipoles can reach 10^{19} m^{-2} in the ballistic regime, which is two orders of magnitude higher than those obtained for graphene on nonferroelectric substrates [14]. The majority of realistic graphene devices are described by the mean free path of electrons ~(50–250) nm and are operating in the diffusive regime. Further, we present the theory of the conductivity of p–n junctions in the graphene channel placed on a ferroelectric substrate caused by a ferroelectric domain wall ub the case of an arbitrary current regime: from the ballistic to diffusive one [15]. It had been demonstrated in [14], [15]] that the graphene channels with pnJ at FDW can serve as excellent rectifiers because of the great ratio of the conductance for the "direct" voltage applied to source and drain electrodes and the "opposite" one caused by the large value of ferroelectric substrate permittivity.

The competition of the absorbed and ferroelectric dipoles would determine the FRAM operation characteristics. We propose a general theory for the analytical description of versatile hysteretic phenomena in a graphene field effect transistor (GFET) allowing for the existence of the external dipoles on the graphene free surface and the localized states at the graphene-surface interface [16]. We have demonstrated that the absorbed dipole molecules (e.g., dissociated or highly polarized water molecules) can cause the hysteretic form of the carrier concentration as a function of the gate voltage and the corresponding dependence of the graphene conductivity in GFET on the substrate of different types, including the most common SiO_2 and ferroelectric ones. Results [16] that are valid for the description of hysteretic phenomena in various realistic GFETs operating at low and intermediate frequency ranges may be not directly applicable for the description of the ferroelectric response at ultra-high frequencies, because the high-frequency response of absorbed and ferroelectric dipoles requires further experimental studies. The results obtained can be useful for the prediction of the most suitable ferroelectric substrates for the graphene-on-ferroelectric-based ultrafast nonvolatile memory of the new generation.

Using a self-consistent approach based on the Landau–Ginzburg–Devonshire phenomenology combined with classical electrostatics, we studied the p–n junctions dynamics in the graphene channel induced by the nucleation, motion, and reversal of stripe domains in a ferroelectric substrate [17]. It is demonstrated that, in the case of intimate electric contact between the ferroelectric and graphene sheet, relatively low gate voltages are required to induce the pronounced hysteresis of the ferroelectric polarization and graphene charge in dependence on the periodic gate voltage. The electric boundary conditions for the polarization at the lateral surfaces of a ferroelectric substrate lead to the asymmetry of the graphene channel conductance between the source and drain electrodes. We have revealed also the pronounced extrinsic size effect in the dependence of the graphene channel conductivity on its length.

The p–n junctions in graphene on FDWs have been actively studied recently, but the role of the piezoelectric effect in a ferroelectric substrate was not considered. We proposed [18] a piezoelectric mechanism of conductance control in the GFET on a ferroelectric substrate with immobile domain walls. In particular, we predicted that the graphene channel conductance can be controlled by the gate voltage due to the piezoelectric elongation and contraction of ferroelectric domains with opposite polarization directions. At the same time, the gate voltage creates the bonded, separated, suspended, and stretched sections of the graphene sheet, whose conductivities and resistivities are significantly different. Our calculations demonstrate the possibility to increase the GFET conductance by several times for ferroelectric substrates with high piezoelectric response. We propose an alternative method of fabrication of suspended graphene areas based on the piezoeffect in a ferroelectric substrate. The method does not require any additional technological procedures like the chemical etching or mechanical treating of the substrate surface.

Taking into account that the conductance of the graphene-on-ferroelectric is significantly higher than the one of graphene on ordinary dielectric substrates, the predicted effect can be very useful for the improvement and miniaturization of many types of electronic devices including various logic elements, memory cells, high-efficiency hybrid electrical modulators, voltage-to-current transducers with frequency doubling and relatively low operation voltages, and piezoresistive elements.

1. K. Novoselov, A. Geim, S. Morozov, D. Jiang, Y. Zhang, S. Dubonos, I. Grigorieva, A. Firsov. Electric Field Effect in Atomically Thin Carbon Films. *Science* **306**, 666 (2004).
2. A. Geim. Graphene: Status and prospects. *Science* **324**, 1530 (2009).
3. S. Das Sarma, Shaffique Adam, E.H. Hwang, E.Rossi. Electronic transport in two-dimensional graphene. *Rev. Mod. Phys.* **83**, 407 (2011).
4. B. Amorim, A. Cortijo, F. de Juan, A.G. Grushin, F. Guinea, A. Gutierrez-Rubio, H. Ochoa, V. Parente, R. Roldan, P. San-Jose, J. Schiefele, M. Sturla, M.A.H. Vozmediano. Novel effects of strains in graphene and other two dimensional materials. *Phys. Rep.* **617**, 1 (2016).
5. G.G. Naumis, S. Barraza-Lopez, M. Oliva-Leyva, H. Terrones. A review of the electronic and optical properties of strained graphene and other similar 2D materials. *arXiv:1611.08627* (2016).
6. Yi Zheng, Guang-Xin Ni, Chee-Tat Toh, Chin-Yaw Tan, Kui Yao, Barbaros Ilzyilmaz. Graphene field-effect transistors with ferroelectric gating. *Phys. Rev. Lett.* **105**, 166602 (2010).
7. Woo Young Kim, Hyeon-Don Kim, Teun-Teun Kim, Hyun-Sung Park, Kanghee Lee, Hyun Joo Choi, Seung Hoon Lee, Jaehyeon Son, Namkyoo Park, Bumki Min. Graphene-ferroelectric metadevices for nonvolatile memory and reconfigurable logic-gate operations. *Nature communications* **7**, Article number: 10429; doi:10.1038/ncomms10429 (2016).
8. X. Hong, J. Hoffman, A. Posadas, K. Zou, C.H. Ahn, J. Zhu. Unusual resistance hysteresis in n-layer graphene field effect transistors fabricated on ferroelectric $Pb(Zr_{0.2}Ti_{0.8})O_3$. *Appl. Phys. Lett.* **97**, 033114 (2010).
9. A. Rajapitamahuni, J. Hoffman, C.H. Ahn, X. Hong. Examining Graphene Field Effect Sensors for Ferroelectric Thin Film Studies. *Nano Lett.* **13**, 4374 (2013).
10. M. Humed Yusuf, B. Nielsen, M. Dawber, X. Du. Extrinsic and intrinsic charge trapping at the graphene/ferroelectric interface. *Nano Lett.* **14** (9), 5437 (2014).
11. J.H. Hinnefeld, R. Xu, S. Rogers, S. Pandya, M. Shim, L.W. Martin, N. Mason. Single Gate PN Junctions in Graphene-Ferroelectric Devices. *arXiv:1506.07138* (2015).
12. C. Baeumer, D. Saldana-Greco, J.M.P. Martirez, A.M. Rappe, M. Shim, L.W. Martin. Ferroelectrically driven spatial carrier density modulation in graphene. *Nature communications* **6**, Article number: 6136; doi:10.1038/ncomms7136 (2015).
13. Jie Wenjing, Jianhua Hao. Time-dependent transport characteristics of graphene tuned by ferroelectric polarization and interface charge trapping. *Nanoscale* (2017). *Nanoscale*, **10**, 328 (2018).
14. A.N. Morozovska, E.A. Eliseev, M.V. Strikha. Ballistic conductivity of graphene channel with *p–n* junction on ferroelectric domain wall. *Appl. Phys. Lett.* **108**, 232902 (2016).
15. M.V. Strikha, A.N. Morozovska. Limits for the graphene on ferroelectric domain wall *p–n*-junction rectifier for different regimes of current. *J. Appl. Phys.* **120**, 214101 (2016).
16. A.I. Kurchak, A.N. Morozovska, M.V. Strikha. Hysteretic phenomena in GFET: general theory and experiment. *J. Appl. Phys.* **122**, 044504 (2017).
17. A.I. Kurchak, E.A. Eliseev, S.V. Kalinin, M.V. Strikha, A.N. Morozovska. *p–n* junctions dynamics in graphene channel induced by ferroelectric domains motion. *Phys. Rev. Appl.* **8**, 024027 (2017).
18. A.N. Morozovska, A.I. Kurchak, M.V. Strikha. Graphene exfoliation at ferroelectric domain wall induced by piezoeffect: impact on the conductance of graphene channel. *Phys. Rev. Appl.* **8**, 054004 (2017).
19. J.R. Williams, L. DiCarlo, C.M. Marcus. Quantum Hall effect in a gate-controlled pn junction of graphene. *Science* **317**, 638 (2007).
20. V. Cheianov, V. Falko. Selective transmission of Dirac electrons and ballistic magnetoresistance of *p–n* junctions in graphene. *Phys. Rev. B* **74**, 041403 (2006).
21. J.R. Whyte, J.M. Gregg. A diode for ferroelectric domainwall motion. *Nature Communications* **6**, Article number: 7361 (2015).
22. N.M. Zhang, M.M. Fogler. Nonlinear screening and ballistic transport in a graphene *p–n* junction. *Phys. Rev. Lett.* **100**, 116804 (2008).
23. Yu.A. Kruglyak, M.V. Strikha. Generalized Landauer – Datta – Lundstrom Model in Application to Transport Phenomena in Graphene. *UJP Reviews* **10**, 3 (2015).
24. C.W. Beenakker. Andreev reflection and Klein tunneling in graphene. *Rev. Mod. Phys.* **80**, 1337 (2008).
25. M.I. Katsnelson, K.S. Novoselov, A.K. Geim. Chiral tunnelling and the Klein paradox in graphene. *Nat. Phys.* **2**, 620 (2006).
26. V. V. Cheianov, V.I. Falko, B.L. Altshuler. The Focusing of Electron Flow and a Veselago Lens in Graphene p-n Junctions. *Science* **315**, 1252 (2007).
27. A.N. Morozovska, M.V. Strikha. Pyroelectric origin of the carrier density modulation at graphene-ferroelectric interface. *J. Appl. Phys.* **114**, 014101 (2013).
28. A.N. Morozovska, E.A. Eliseev, A.V. Ievlev, O.V. Varenyk, A.S. Pusenkova, Ying-Hao Chu, V.Ya. Shur, M.V. Strikha, S.V. Kalinin. Ferroelectric domain triggers the charge modulation in semiconductors. *J. Appl. Phys.* **116**, 066817 (2014).
29. I.I. Naumov, A.M. Bratkovsky. Gap opening in graphene by simple periodic inhomogeneous strain. *Phys. Rev. B* **84**, 245444 (2011).
30. T.L. Linnik. Effective Hamiltonian of strained graphene. *J. Phys.: Condens. Matter* **24**, 205302 (2012).
31. T.L. Linnik. Photoinduced valley currents in strained graphene. *Phys. Rev. B* **90**, 075406 (2014).
32. E.A. Eliseev, A.N. Morozovska, S.V. Kalinin, Y.L. Li, Jie Shen, M.D. Glinchuk, L.Q. Chen, V. Gopalan. Surface Effect on Domain Wall Width in Ferroelectrics. *J. Appl. Phys.* **106**, 084102 (2009).

33. V. Cheianov, V. Falko. Selective transmission of Dirac electrons and ballistic magnetoresistance of n–p junctions in graphene. *Phys. Rev. B* **74**, 041403 (2006).
34. A.N. Morozovska, A.S. Pusenkova, O.V. Varenyk, S.V. Kalinin, E.A. Eliseev, M.V. Strikha. Finite size effects of hysteretic dynamics in multi-layer graphene on ferroelectric. *Phys. Rev. B* **91**, 235312 (2015).
35. S. Datta. *Lessons from nanoelectronics: A new perspective on transport* (Hackensack, World Scientific Publishing Company, 2015).
36. D. Singh, J.Y. Murthy, T.S. Fisher. Mechanism of thermal conductivity reduction in few-layer graphene. *J. Appl. Phys.* **110** 094312 (2011).
37. A.K. Tagantsev, L.E. Cross, J. Fousek. *Domains in ferroic crystals and thin films* (Springer, 2010) [ISBN: 978-1-4419-1416-3].
38. Y.O. Krugliak, M.V. Strihka. Generalized landauer–datta–lundstrom model in application to transport phenomena in graphene. *Ukr. J. Phys. Reviews* **10**, 3 (2015).
39. M.V. Strikha. Mechanism of the antihysteresis behavior of the resistivity of graphene on a $Pb(Zr_xTi_{1-x})O_3$ ferroelectric substrate. *JETP Letters* **95**, 198 (2012).
40. A.I. Kurchak, M.V. Strikha. Antihysteresis of the electrical resistivity of graphene on a ferroelectric $Pb(Zr_xTi_{1-x})O_3$ substrate. *JETP* **143**, 129 (2013).
41. A.K. Tagantsev, L.E. Cross, J. Fousek. *Domains in Ferroic Crystals and Thin Films* (Springer, 2010).
42. A.I. Kurchak, A.N. Morozovska, M.V. Strikha. Rival mechanisms of hysteresis in the resistivity of graphene channel. *Ukr. J. Phys.* **58**, 472 (2013).
43. Y. Zheng, G.-X. Ni, C.-T. Toh, C.-Y. Tan, K. Yao, B. Ozyilmaz. Graphene field-effect transistors with ferroelectric gating. *Phys. Rev. Lett.* **105**, 166602 (2010).
44. L.D. Landau, I.M. Khalatnikov. On the anomalous absorption of sound near a second order phase transition point. *Dokl. Akad. Nauk SSSR* **96**, 469–472 (1954).
45. S.V. Kalinin, A.N. Morozovska, L.Q. Chen, B.J. Rodriguez. Local polarization dynamics in ferroelectric materials. *Rep. Prog. Phys.* **73**, 056502-1-67 (2010).
46. H. Wang, Y. Wu, C. Cong, J. Shang, T. Yu. Hysteresis of Electronic Transport in Graphene Transistors. *ACS Nano* **4**, 7221 (2010).
47. M. Lafkioti, B. Krauss, T. Lohmann, U. Zschieschang, H. Klauk, K. Klitzing, J.H. Smet. Graphene on a hydrophobic substrate: doping reduction and hysteresis suppression under ambient conditions. *Nano Lett.* **10**, 1149 (2010).
48. A. Veligura, P.J. Zomer, I.J. Vera-Marun, C. Jyzsa, P.I. Gordiichuk, B.J. van Wees. Relating hysteresis and electrochemistry in graphene field effect transistors *J. Appl. Phys.* **110**, 113708 (2011).
49. M.V. Strikha. Non volatile memory of new generation and ultrafast IR modulators based on graphene on ferroelectric substrate. In: *Functional Nanomaterials and Devices for Electronics, Sensors and Energy Harvesting.* Ed. by A. Nazarov, F. Balestra, V. Kilchytska, D. Flandre (Springer International Publishing, 2014).
50. M.V. Strikha. Hysteresis in the resistivity of graphene channel. In: *Chemical Functionalization of Carbon Nanomaterials: Chemistry and Application.* Ed. by V.K. Thakur, M.K. Thakur (Taylor and Francis, 2015).
51. C. Baeumer, S.P. Rogers, R. Xu, L.W. Martin, M. Shim. Tunable carrier type and density in graphene/$PbZr_{0.2}Ti_{0.8}O_3$ hybrid structures through ferroelectric switching. *Nano Letters.* **13**, 1693 (2013).
52. S.S. Sabri, P.L. Levesque, C.M. Aguirre *et al. Appl. Phys. Lett.* **95**, 242104 (2009).
53. H. Wang, Y. Wu, C. Cong *et al. ACS Nano* **4**, 7221 (2010).
54. A. Veligura, P.J. Zomer, I.J. Vera-Marun *et al. J. Appl. Phys.* **110**, 113708 (2011).
55. A.K. Tagantsev, G. Gerra. Interface-induced phenomena in polarization response of ferroelectric thin films. *J. Appl. Phys.* **100**, 051607 (2006).
56. A. K. Tagantsev, M. Landivar, E. Colla, and N. Setter. Identification of passive layer in ferroelectric thin films from their switching parameters. *J. Appl. Phys.* **78**, 2623 (1995).
57. G. Rupprecht, R.O. Bell. Dielectric constant in paraelectric perovskite. *Phys. Rev.* **135**, A748 (1964).
58. E.J.G. Santos. Electric Field Effects on Graphene Materials. In *Exotic Properties of Carbon Nanomatter* (Springer, 2015), pp. 383–391.
59. J. Hlinka, P. Márton. Phenomenological model of a 90° domain wall in $BaTiO_3$-type ferroelectrics. *Phys. Rev. B* **74**, 104104 (2006).
60. L.D. Landau, I.M. Khalatnikov. On the anomalous absorption of sound near a second order phase transition point. *Dokl. Akad. Nauk SSSR* **96**, 469 (1954).
61. R. Kretschmer, K.Binder. Surface effects on phase transitions in ferroelectrics and dipolar magnets. *Phys. Rev. B* **20**, 1065 (1979).
62. Chun-Lin Jia, Valanoor Nagarajan, Jia-Qing He, Lothar Houben, Tong Zhao, Ramamoorthy Ramesh, Knut Urban, Rainer Waser. Unit-cell scale mapping of ferroelectricity and tetragonality in epitaxial ultrathin ferroelectric films. *Nature Materials* **6**, 64 (2007).
63. A.N. Morozovska, E.A. Eliseev, N.V. Morozovsky, S.V. Kalinin. Ferroionic states in ferroelectric thin films. *Phys. Rev. B* **95**, 195413 (2017).
64. E.A. Eliseev, A.N. Morozovska. General approach to the description of the size effect in ferroelectric nanosystems. *The Journal of Materials Science.* **44** (19), 5149 (2009).
65. A.N. Morozovska, E.A. Eliseev, S.V. Svechnikov, A.D. Krutov, V.Y. Shur, A.Y. Borisevich, P. Maksymovych, S.V. Kalinin. Finite size and intrinsic field effect on the polar-active properties of ferroelectric semiconductor heterostructures. *Phys. Rev. B* **81**, 205308 (2010).
66. A.K. Tagantsev, L.E. Cross, J. Fousek. *Domains in Ferroic Crystals and Thin Films* (Springer, 2010) [ISBN: 978-1-4419-1416-3].
67. M.J. Haun, E. Furman, S.J. Jang, L.E. Cross. Thermodynamic theory of the lead zirconate-titanate solid solution

system, Part V: Theoretical calculations. *Ferroelectrics* **99**, 63 (1989) (see figure 16 and table I).
68. S.P. Koenig, N.G. Boddeti, M.L. Dunn, J.S. Bunch. Ultrastrong adhesion of graphene membranes. *Nature Nanotechnology* **6**, 543 (2011).
69. A. Politano, G. Chiarello. Probing the Young's modulus and Poisson's ratio in graphene/metal interfaces and graphite: A comparative study. *Nano Research* **8** (6), 1847 (2015).
70. T. Chen, R. Cheung. Mechanical Properties of Graphene. In: *Graphene Science Handbook. Mechanical and Chemical Properties* (CRC Press, 2016).
71. F. Felten, G.A. Schneider, J. Mucoz Saldaca, S.V. Kalinin. Modeling and measurement of surface displacements in $BaTiO_3$ bulk material in piezoresponse force microscopy. *J. Appl. Phys.* **96** (1), 563 (2004).
72. S.V. Kalinin, E.A. Eliseev, A.N. Morozovska. Materials contrast in piezoresponse force microscopy. *Appl. Phys. Lett.* **88**, (23) (2006).
73. A.N. Morozovska, E.A. Eliseev, S.L. Bravina, S.V. Kalinin. Resolution function theory in piezoresponse force microscopy: Domain wall profile, spatial resolution, and tip calibration. *Phys. Rev. B* **75** (17), 174109 (2007).
74. S.V. Kalinin, A.N. Morozovska, L.Q. Chen, B.J. Rodriguez. Local polarization dynamics in ferroelectric materials. *Reports on Progress in Physics* **73** (5), 056502 (2010).
75. S.V. Kalinin, B.J. Rodriguez, S.-H. Kim, S.-K. Hong, A. Gruverman, E.A. Eliseev. Imaging Mechanism of Piezoresponse Force Microscopy in Capacitor Structures. *Appl. Phys. Lett.* **92**, 152906 (2008).
76. J.S. Bunch, A.M. van der Zande, S.S. Verbridge, I.W. Frank, D.M. Tanenbaum, J.M. Parpia, H.G. Craighead, P.L. McEuen. Electromechanical resonators from graphene sheets. *Science* **315**, 490 (2007).
77. N. Levy, S.A. Burke, K.L. Meaker, M. Panlasigui, A. Zettl, F. Guinea, A.H. Castro Neto, M.F. Crommie. Strain – induced pseudo – magnetic fields greater than 300 tesla in graphene nanobubbles. *Science* **329**, 544 (2010).

Received 01.12.17

А.І. Курчак

ВПЛИВ ДОМЕННОЇ СТРУКТУРИ СЕГНЕТОЕЛЕКТРИЧНОЇ ПІДКЛАДКИ НА ПРОВІДНІСТЬ ГРАФЕНУ

Р е з ю м е

Огляд присвячено останнім теоретичним дослідженням впливу доменної структури сегнетоелектричної підкладки на провідність графенового каналу. Розглянутий аналітичний опис ефектів пам'яті гістерезисного типу у польовому транзисторі на основі графен-на-сегнетоелектрику, з урахуванням адсорбованих дипольних шарів на вільній поверхні графену і локалізованих станів на його інтерфейсах. Аналізуються аспекти нещодавно розвинутої теорії провідності p–n переходів у графеновому каналі на сегнетоелектричній підкладці, які створені 180-градусною сегнетоелектричною доменною структурою, причому розглянуті випадки різних режимів струму, від балістичного до дифузійного. Обговорюється вплив розмірних ефектів у таких системах та можливість використання результатів для вдосконалення характеристик польових транзисторів з графеновим каналом, комірок енергонезалежної сегнетоелектричної пам'яті з довільним доступом, сенсорів, а також для мініатюризації різних пристроїв функціональної наноелектроніки